

See discussions, stats, and author profiles for this publication at: <https://www.researchgate.net/publication/257942360>

# Geologically constraining India in Columbia: The age, isotopic provenance and geochemistry of the protoliths of the Ongole Domain, Southern Eastern Ghats, India

ARTICLE *in* GONDWANA RESEARCH · SEPTEMBER 2013

Impact Factor: 8.24 · DOI: 10.1016/j.gr.2013.09.002

---

CITATIONS

12

READS

165

---

## 5 AUTHORS, INCLUDING:



[Bonnie Henderson](#)  
University of Adelaide  
5 PUBLICATIONS 13 CITATIONS

[SEE PROFILE](#)



[Alan Stephen Collins](#)  
University of Adelaide  
152 PUBLICATIONS 5,460 CITATIONS

[SEE PROFILE](#)



[Caroline J Forbes](#)  
University of Adelaide  
13 PUBLICATIONS 209 CITATIONS

[SEE PROFILE](#)



[Dilip Saha](#)  
Indian Statistical Institute  
40 PUBLICATIONS 426 CITATIONS

[SEE PROFILE](#)



Contents lists available at ScienceDirect

## Gondwana Research

journal homepage: [www.elsevier.com/locate/gr](http://www.elsevier.com/locate/gr)

# Geologically constraining India in Columbia: The age, isotopic provenance and geochemistry of the protoliths of the Ongole Domain, Southern Eastern Ghats, India

Bonnie Henderson <sup>a,\*</sup>, Alan S. Collins <sup>a</sup>, Justin Payne <sup>a</sup>, Caroline Forbes <sup>a</sup>, Dilip Saha <sup>b</sup><sup>a</sup> Tectonics Resources and Exploration (TRaX), School of Earth and Environmental Sciences, The University of Adelaide, Adelaide, SA 5005, Australia<sup>b</sup> Geological Studies Unit (GSU), Indian Statistical Institute, Kolkata, India

## ARTICLE INFO

## Article history:

Received 7 May 2013

Received in revised form 23 August 2013

Accepted 6 September 2013

Available online xxxx

Handling Editor: M. Santosh

## Keywords:

Ongole Domain

Eastern Ghats

Nuna

Columbia

India

## ABSTRACT

The Ongole Domain in the southern Eastern Ghats Belt of India formed during the final stages of Columbia amalgamation at ca. 1600 Ma. Yet very little is known about the protolith ages, tectonic evolution or geographic affinity of the region. We present new detrital and igneous U-Pb-Hf zircon data and in-situ monazite data to further understand the tectonic evolution of this Columbia-forming orogen.

Detrital zircon patterns from the metasedimentary rocks are dominated by major populations of Palaeoproterozoic grains (ca. 2460, 2320, 2260, 2200–2100, 2080–2010, 1980–1920, 1850 and 1750 Ma), and minor Archaean grains (ca. 2850, 2740, 2600 and 2550 Ma). Combined U-Pb ages and Lu-Hf zircon isotopic data suggest that the sedimentary protoliths were not sourced from the adjacent Dharwar Craton. Instead they were likely derived from East Antarctica, possibly the same source as parts of Proterozoic Australia. Magmatism occurred episodically between 1.64 and 1.57 Ga in the Ongole Domain, forming felsic orthopyroxene-bearing granitoids. Isotopically, the granitoids are evolved, producing εHf values between –2 and –12. The magmatism is interpreted to have been derived from the reworking of Archaean crust with only a minor juvenile input. Metamorphism between 1.68 and 1.60 Ga resulted in the partial to complete resetting of detrital zircon grains, as well as the growth of new metamorphic zircon at 1.67 and 1.63 Ga. In-situ monazite geochronology indicates metamorphism occurred between 1.68 and 1.59 Ga.

The Ongole Domain is interpreted to represent part of an exotic terrane, which was transferred to proto-India in the late Palaeoproterozoic as part of a linear accretionary orogenic belt that may also have included south-west Baltica and south-eastern Laurentia. Given the isotopic, geological and geochemical similarities, the proposed exotic terrane is interpreted to be an extension of the Napier Complex, Antarctica, and may also have been connected to Proterozoic Australia (North Australian Craton and Gawler Craton).

© 2013 International Association for Gondwana Research. Published by Elsevier B.V. All rights reserved.

## 1. Introduction

The late Palaeoproterozoic to Mesoproterozoic transition (ca. 1.7–1.5 Ga) from the supercontinent Columbia (also known variously as Nuna, Rogers and Santosh, 2002; Hou et al., 2008; Evans and Mitchell, 2011) to the supercontinent Rodinia is a time of relative quiescence in the core Nuna continents of Laurentia, Siberia and Baltica (Swain et al., 2005; Hollis et al., 2010). Robust palaeopolises from Laurentia and Baltica between ca. 1780 and 1740, 1480 and 1460 and 1270 and 1260, and from Laurentia and Siberia at 1480–1460 Ma suggest that they may have represented a single continental mass between ca. 1500 and 1270 Ma (Hollis et al., 2010). The reconfiguration of the three continents into Rodinia is apparently limited to relatively small continental separations and rotations around local

poles (Evans and Mitchell, 2011; Zhang et al., 2012). It has been difficult to include other major Proterozoic continents, such as the Australian, Indian, South American and East Asian continents into Columbia supercontinent reconstructions due to the relative lack of geological and palaeomagnetic data. However, a new palaeomagnetically-constrained reconstruction of Columbia includes both India and Australia in Columbia and locates them securely in an intracontinental position in the core of Columbia throughout the Palaeo-Mesoproterozoic (Zhang et al., 2012). This position is somewhat controversial as the period between 1.7 and 1.5 Ga is a time of considerable magmatism, metamorphism, and crustal orogenesis within Australia (Betts and Giles, 2006; Cawood and Korsch, 2008) and India (Dobmeier and Raith, 2003; Bhowmik and Dasgupta, 2012), which has been linked to active margin settings.

To better understand the nature of this ancient supercontinent transition, and examine the role of India within it, we investigate the evolution of the Ongole Domain, India. The Ongole Domain is a region of granulite-facies metasedimentary and igneous rocks in the southern Eastern Ghats Belt (Dobmeier and Raith, 2003). This region is suggested

\* Corresponding author at: Mawson Laboratories, University of Adelaide, North Terrace, 5005, SA, Australia. Tel.: +61 8 8313 4971.

E-mail address: [bonnie.henderson@adelaide.edu.au](mailto:bonnie.henderson@adelaide.edu.au) (B. Henderson).

to have played an integral role in the assembly of the supercontinent Columbia; specifically during a tectonothermal event at *ca.* 1.6 Ga that sutured the Ongole Domain with proto-India and possibly the Napier Complex in East Antarctica (Ravikant, 2010; Bose et al., 2011; Vijaya Kumar et al., 2011). We present new U-Pb, Lu-Hf and trace element data for detrital and igneous zircons, as well as in-situ monazite geochronology to characterise the provenance and timing of sedimentary protolith deposition, timing of magmatism and timing of metamorphism from the Ongole Domain. These data are used to propose a new model for the late Palaeoproterozoic tectonic evolution of eastern India.

## 2. Geological background

The Eastern Ghats Belt (EGB) is a multiply deformed, granulite-facies orogen that trends NW-SE along the south-eastern coast of India for approximately 1000 km (Fig. 1A). The EGB is divided into four provinces, the Jeypore Province, Rengali Province, Eastern Ghats Province (EGP) and the Krishna Province, each characterised by distinct tectonothermal histories (Ramakrishnan et al., 1998; Rickers et al., 2001; Dobmeier and Raith, 2003). The oldest provinces, the Jeypore and Rengali (Fig. 1B), are suggested to have either accreted to proto-India prior to the *ca.* 1000 Ma assembly of Rodinia (Mukhopadhyay and Basak, 2009), or to be thoroughly reworked fragments of the Archaean-aged eastern Dharwar Craton (Ramakrishnan and Vaidyanadhan, 2010). The centrally located EGP (Fig. 1B) forms the most extensive province and underwent ultra high temperature (UHT) metamorphism and orogenesis at *ca.* 980–930 Ma, during the amalgamation of Rodinia (Korhonen et al., 2011). The Krishna Province (Fig. 1B) records collisional orogenesis and high temperature metamorphism at *ca.* 1600 Ma (Dobmeier and Raith, 2003; Naqvi, 2005; Upadhyay et al., 2009), but shows very little evidence of the pervasive Neoproterozoic orogenesis seen further north in the EGP (Mezger and Cosca, 1999a; Dobmeier et al., 2006).

The Krishna Province is further subdivided into the granulite-facies Ongole Domain in the east, and the low to medium grade Nellore Schist Belt (NSB) in the west (Fig. 1B). The NSB is juxtaposed against the eastern margin of the Cuddapah Basin along the Vellikonda thrust front (Saha, 2011); a major intracontinental thrust that accommodated significant upper crustal shortening during protracted events that accreted the NSB and EGP to the Eastern Dharwar Craton (Saha, 2011). The NSB

consists of metamorphosed volcano-sedimentary pelites and psammites that increase in metamorphic grade from greenschist to upper amphibolites facies towards the east. U-Pb zircon ages of  $1868 \pm 6$  Ma and  $1771 \pm 8$  Ma constrain the timing of andesite and felsic volcanism respectively in the NSB (Vadlamani et al., 2012). Layered gabbro-anorthosite complexes within the NSB have yielded Nd model ages of *ca.* 1170 Ma and have been interpreted as representing the roots of a volcanic arc (Dharma Rao et al., 2011b). However, the geochemical evidence quoted for an arc origin (negative Nb and Ti anomalies) is not supported by the data they present. Along the south eastern boundary of the NSB, thrust faults, ophiolites and tectonic mélange have been interpreted as fragments of Proterozoic sutures, which separate the NSB from the Ongole Domain (Kumar and Leelanandam, 2008; Dharma Rao and Reddy, 2009; Kumar et al., 2010; Dharma Rao et al., 2011a).

The Ongole Domain (Fig. 1B) is comprised of predominantly mafic and plutonic felsic granulites that often include hypersphene-bearing charnockites, enderbites or leucocratic orthogneiss interlayered with porphyritic leptynites (Dobmeier and Raith, 2003). Zircon U-Pb isotope data from charnockites and enderbites yield crystallisation ages between *ca.* 1720 and 1700 Ma (Kovach et al., 2001). The same rocks yield Nd depleted mantle model ages of 2.5–2.3 Ga (Rickers et al., 2001). Anorthosite, gabbronorite and pyroxenite emplacement in the Pangidi-Kondapalle Complex within the central Ongole Domain has been dated at *ca.* 1630 Ma (Dharma Rao et al., 2012), and granite emplacement at Vinukonda in the south has been dated at *ca.* 1590 Ma (Dobmeier et al., 2006). Mineralogical and geochemical data from the Kondapalle Complex were interpreted to mean that these rocks represent the root zone of a deeply eroded late Palaeoproterozoic (~1630 Ma) continental magmatic arc (Dharma Rao and Santosh, 2011). Metasedimentary rocks are rare in the Ongole Domain, and are exposed mostly in the east, as partly assimilated layers within the intrusive igneous bodies (Dobmeier and Raith, 2003). The timing of deposition and provenance of the metasedimentary protoliths are poorly known. Nd isotope data from the metasedimentary rocks yield Nd depleted mantle model ages ( $T_{DMC}$ ) of 2.8 to 2.6 Ga. This has been interpreted to indicate derivation of the sedimentary protolith rocks from the abundant granitoids of similar age in the eastern Dharwar Craton (Rickers et al., 2001).

Reported ages for metamorphism in the Ongole Domain are variable. Laser Inductively Coupled Mass Spectrometry (LA-ICP-MS) U-Pb zircon

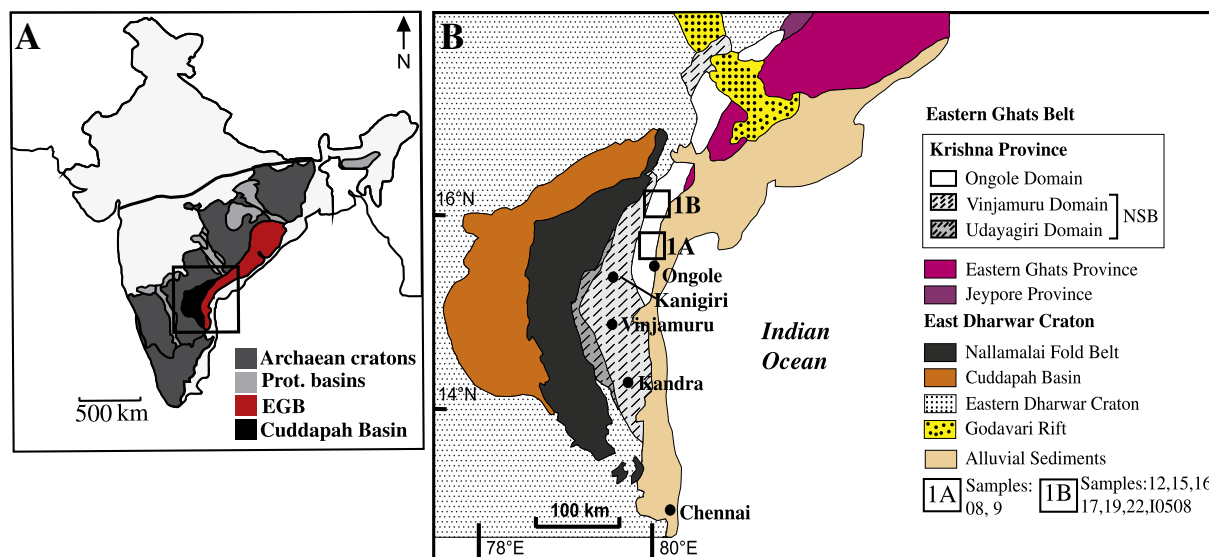


**Fig. 1.** A. Simplified geological map of India showing the location of the Eastern Ghats Belt, Cuddapah Basin, Archaean Cratons and other Proterozoic basins. Modified after French et al. (2008). B. Geological map showing the location of the southern Eastern Ghats Belt; Highlights the subdivision of the Krishna Province into individual domains (Ongole Domain, Vinjamuru Domain and the Udayagiri Domain). Sample locations from Area 1A and Area 1B are shown in the boxes (1A & 1B). Figure modified from Dobmeier et al. (2006).

data from metapelitic rocks produced concordant ages of *ca.* 1630 Ma for cores and *ca.* 1610 Ma for rims ([Upadhyay et al., 2009](#)). Weak cathodoluminescence, and a lack of internal zonation in the zircon grains, were used as evidence to suggest isotopic resetting during UHT metamorphism at *ca.* 1630–1610 Ma ([Upadhyay et al., 2009](#)). Monazite grains from metasedimentary rocks yielded four peak ages at *ca.* 3450, 2500, 1580 and 1480 Ma ([Simmat and Raith, 2008](#)); whereby the two older populations were interpreted to be detrital and the *ca.* 1580 Ma grains were suggested to constrain the timing of UHT metamorphism. The *ca.* 1480 Ma monazite grains were interpreted to have recrystallised during localised ductile to brittle deformation in the late Mesoproterozoic ([Simmat and Raith, 2008; Upadhyay et al., 2009](#)). Conversely, petrological investigations have also identified an earlier, possible UHT, event ([Sengupta et al., 1999](#)), which was suggested to have occurred at *ca.* 1760 Ma ([Bose et al., 2011](#)). Alkaline intrusions post-date the *ca.* 1700–1600 Ma tectonothermal magmatic event with prolonged alkaline magmatism recorded in the Prakasam Alkaline Complex between *ca.* 1370 and 1100 Ma ([Sarkar and Paul, 1998](#)).

The recognition of oceanic sutures located between the NSB and the Ongole Domain (e.g. at Kandra and Kanigiri, Fig. 1B) has been used to suggest the presence of an active continental margin during the Palaeo-Mesoproterozoic ([Kumar et al., 2010; Dharma Rao and Santosh, 2011; Dharma Rao et al., 2011a](#)). Recent U-Pb zircon data from the interpreted suture zones record crystallisation ages of *ca.* 1850 Ma from two sheeted dolerite dykes within the Kandra Ophiolite Complex ([Kumar et al., 2010](#)) and *ca.* 1330 Ma for four granites and two gabbro samples from the Kanigiri Ophiolite Melange ([Dharma Rao et al., 2011a](#)). [Dharma Rao et al. \(2011a\)](#) used these ages to suggest the presence of a subduction zone along the eastern coast of India, active for at least 500 Ma (*ca.* 1850–1330 Ma), where multiple generations of oceanic crust were accreted to the Indian margin. Geochemical analyses of the metabasalts, wherlites and serpentinites support the possibility of an ophiolitic melange at Kanigiri ([Dharma Rao and Reddy 2009](#)). However, no supporting geochemical data has been published for the dated granites. As granitic material volumetrically dominates the region, there is the alternative possibility that the dates are associated with emplacement of the un-foliated, post-tectonic granitoids previously reported in the area ([Simmat and Raith, 1998](#)). [Vijaya Kumar et al. \(2010, 2011\)](#) provide a contrasting tectonic model in which the Kandra Ophiolite Complex represents a continental backarc basin formed during subduction rollback at 1.85 Ga, which was subsequently emplaced over the eastern Dharwar Craton immediately after its formation, or during terminal collision at *ca.* 1.6 Ga. In a recent review [Dasgupta et al. \(2013\)](#) propose an evolutionary model for the southern eastern Ghats Belt that encompasses all available geochemical,

geochronological and geological data. Their model favours that proposed by [Vijaya Kumar et al. \(2010, 2011\)](#), and caution against assigning tectonic implications to post-1.60 Ga events due to the current lack of petrological support.

### 3. Analytical methods

Based on the level and quality of exposed outcrop in the Ongole Domain, two areas were targeted for sampling (Fig. 2). The first area (Area 1A) is located in the south east of the Ongole Domain, and the second (Area 1B) is situated approximately 70 km north of Domain 1 (Fig. 2). Typical pelitic assemblages incorporating biotite, garnet, sillimanite, cordierite and quartz were targeted for provenance studies of the sedimentary protoliths. The location, mineralogy and interpreted protolith to each of the samples are listed in Table 1.

#### 3.1. U-Pb zircon geochronology

Analytical techniques for U-Pb isotopic dating of zircon and monazite follow those of [Payne et al. \(2008, 2010\)](#). Samples chosen for zircon geochronology were crushed using a jaw crusher, sieved to obtain a size fraction between 75 and 425 µm. Traditional hand panning techniques, conventional magnet techniques and Frantz Isodynamic separation and heavy liquid separation (methylene iodide) were used to separate zircon from the sieved crushate. Approximately 200 zircon grains per sample were handpicked and mounted in epoxy resin. Prior to analysis, zircon grains were imaged at Adelaide Microscopy, The University of Adelaide, using a Phillips XL20 SEM with attached Gatan cathodoluminescence (CL) detector.

U-Th-Pb analysis of zircons was also conducted at Adelaide Microscopy, using an Agilent 7500cs ICPMS, coupled to a New Wave 213 nm Nd-YAG laser. U-Pb fractionation was corrected using the GEMOC GJ-1 zircon (TIMS normalisation data  $^{207}\text{Pb}/^{206}\text{Pb} = 608.3$  Ma,  $^{206}\text{Pb}/^{238}\text{U} = 600.7$  Ma and  $^{207}\text{Pb}/^{235}\text{U} = 602.2$  Ma; [Jackson et al., 2004](#)). A second zircon standard (Plesovice, TIMS-ID U-Pb age:  $337.1 \pm 0.4$  Ma, [Sláma et al., 2008](#)) – was used to monitor the ongoing accuracy of the instrument. Data reduction was completed using the program “GLITTER” ([Griffin et al., 2008](#)). Weighted average calculations use  $^{207}\text{Pb}/^{206}\text{Pb}$  ages for zircon populations older than 1000 Ma and  $^{206}\text{Pb}/^{238}\text{U}$  ages for those populations younger than 1000 Ma. A  $\pm 10\%$  discordancy threshold was applied to zircon analysis during age interpretation. GJ-1 produced a weighted average  $^{206}\text{Pb}/^{238}\text{U}$  age of  $600.48 \pm 0.92$  Ma ( $n = 270$ , MSWD = 0.83), and Plesovice a  $^{206}\text{Pb}/^{238}\text{U}$  age weighted average of  $337.9 \pm 1.6$  Ma ( $n = 73$ , MSWD = 2.1).

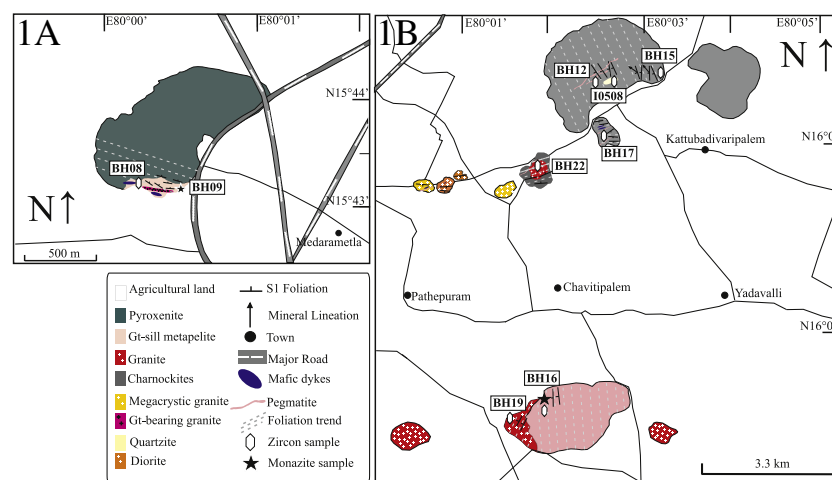


**Fig. 2.** Simplified location map from area 1A and 1B showing the exposed geology and the location of zircon and monazite samples. Also shown are the locations of felsic pegmatites and mafic dykes. N.B. The foliation preserved in the oldest rocks in the two areas (BH12, BH15, BH16, BH19) strikes roughly N-S, whereas the younger rocks (BH22, BH17) strikes roughly E-W.

**Table 1**

Sample locations, mineralogy, lithology and interpreted protolith rock for each of the samples from the Ongole Domain. Mineral abbreviations as defined by Kretz (1983).

Sample ID	Northing	Easting	Mineral Assemblage	Lithology	Interpreted Protolith
BH08	15°43'81.9"	80°00'48.5"	gt + qtz + sill + cd + kfs + ilm + mag + bi	Gt - sill - cd gneiss	Sedimentary
BH09	15°43'81.9"	80°00'48.5"	gt + qtz + sill + cd + kfs + ilm + mag + bi	Gt - sill - cd gneiss	Sedimentary
BH12	16°08'72.0"	80°02'03.7"	kfs + qtz + perth + pl + opx + bi + mag	Charnockite	Igneous
BH15	16°08'90.1"	80°02'92.8"	kfs + qtz + perth + pl + cpx + opx + mag + bi	Charnockite	Igneous
BH16	16°04'46.4"	80°04'40.4"	gt + opx + ilm + pl + kfs + perth + bi	Gt-opx gneiss	Sedimentary
BH17	16°08'11.1"	80°02'14.6"	kfs + qtz + perth + pl + cpx + opx + mag + bi	Charnockite	Igneous
BH19	16°01'20.4"	80°01'18.6"	qtz + pl + perth + bi	Granite	Igneous
BH22	16°01'41.0"	80°01'16.3"	qtz + perth + plg + bi + hbl	Quartz-monzonite	Igneous
I0508	16°08'24.5"	80°01'45.4"	qtz + perth + sill + ilm	Quartzite	Sedimentary

### 3.2. Monazite geochronology

In-situ U-Pb analysis of monazites was also conducted at Adelaide Microscopy, also using the Agilent 7500cs ICPMS coupled with the New Wave 213 nm Nd-YAG laser. Analytical techniques for U-Pb isotopic dating of monazite grains follow those of Payne et al. (2008). In-situ monazite grains were identified and imaged on thin sections for samples BH09 and BH16, using the Phillips XL30 SEM with a Backscattered Electron detector (BSE). This technique allows for the textural relationship of the monazite grains with other minerals to be recorded.

U-Pb fractionation was corrected using the documented standard Madel (Payne et al., 2008), in conjunction with the in-house standard 222 (Maidment et al., 2005), which was used to monitor ongoing accuracy of the laser. Data reduction was completed using GLITTER software (Van Achterbergh et al., 2001). A ± 5% discordancy threshold was applied to zircon analysis during age interpretation. The weighted average  $^{206}\text{Pb}/^{238}\text{U}$  age for Madel is  $516.2 \pm 2.0$  ( $n = 51$ , MSWD = 0.92), and the weighted average  $^{206}\text{Pb}/^{238}\text{U}$  age for 222 is  $455.6 \pm 5.6$  Ma ( $n = 16$ , MSWD = 1.6).

### 3.3. Lu-Hf isotopic analysis

The zircon mounts prepared for U-Pb LA-ICPMS analysis were also used for Lu-Hf isotopic studies undertaken with Laser Ablation Multi-Collector Inductively Coupled Plasma Mass Spectrometry (LA-MC-ICPMS) at the Waite campus, University of Adelaide, South Australia. Only grains with U-Pb LA-ICPMS analysis greater than 95% concordance were analysed for Lu-Hf isotope composition. Analysis spots were placed as close as possible to concordant U-Pb LA-ICPMS spots, and within the same CL zone. Zircons were ablated with a New Wave UP-193 Excimer laser (193 nm) using a spot size of  $50 \mu\text{m}$ , frequency of 5 Hz, 4 ns pulse length and an intensity of  $\sim 10 \text{ J/cm}^2$ . Zircons were ablated in a helium atmosphere, which was then mixed with argon upstream of the ablation cell. Measurements were made using a Thermo-Scientific Neptune Multi Collector ICP-MS equipped with Faraday detectors and  $10^{11} \Omega$  amplifiers. Analyses used a dynamic measurement routine with: ten 0.524 s integrations on  $^{171}\text{Yb}$ ,  $^{173}\text{Yb}$ ,  $^{175}\text{Lu}$ ,  $^{176}\text{Hf}$  (+ Lu + Yb),  $^{177}\text{Hf}$ ,  $^{178}\text{Hf}$ ,  $^{179}\text{Hf}$  and  $^{180}\text{Hf}$ ; one 0.524 s integration on  $^{160}\text{Gd}$ ,  $^{163}\text{Dy}$ ,  $^{164}\text{Dy}$ ,  $^{165}\text{Ho}$ ,  $^{166}\text{Er}$ ,  $^{167}\text{Er}$ ,  $^{168}\text{Er}$ ,  $^{170}\text{Yb}$  and  $^{171}\text{Yb}$ , and one 0.524 s integration of Hf oxides with masses ranging from 187 to 196 amu. An idle time of 1.5 s was included between each mass change to allow for magnet settling and to negate any potential effects of signal decay. This measurement cycle is repeated 15 times to provide a total maximum measurement time of 3.75 min including an off-peak baseline measurement. The measurement routine is optimised to allow for the monitoring of oxide formation rates and REE content of zircon, and to provide the option to correct for REE-oxide interferences if required in high REE zircon. Hf oxide formation rates for all analytical sessions in this study were in the range 0.1–0.07%.

Hf mass bias was corrected using an exponential fractionation law with a stable  $^{179}\text{Hf}/^{177}\text{Hf}$  ratio of 0.7325. Yb and Lu isobaric interferences on  $^{176}\text{Hf}$  were corrected for following the methods of Woodhead et al.

(2004).  $^{176}\text{Yb}$  interference on  $^{176}\text{Hf}$  was corrected for by direct measurement of Yb fractionation using measured  $^{171}\text{Yb}/^{173}\text{Yb}$  with the Yb isotopic values of Segal et al. (2003). The applicability of these values were verified by analysing JMC 475 Hf solutions doped with varying levels of Yb with interferences up to  $^{176}\text{Yb}/^{177}\text{Hf} = \sim 0.5$ . Lu isobaric interference on  $^{176}\text{Hf}$  was corrected using a  $^{176}\text{Lu}/^{175}\text{Lu}$  ratio of 0.02655 (Vervoort et al., 2004) assuming the same mass bias behaviour as Yb.

Confirmation of accuracy of the technique was monitored using a combination of the Plesovice, Mudtank and QGNG zircon standards. The average  $^{176}\text{Hf}/^{177}\text{Hf}$  value for Plesovice for the analytical session was  $0.282479 \pm 0.000022$  (2SD,  $n = 27$ ), which is comparable to the published value of  $0.282482 \pm 0.000013$  (2SD) by Sláma et al. (2008).

$\epsilon\text{Hf}_{(T)}$ ,  $T_{\text{DMc}}$  and  $T_{\text{DMc}}$  crustal were calculated using  $^{176}\text{Lu}$  decay constant after Scherer et al. (2001).  $T_{\text{DMc}}$  crustal was calculated using the methods of Griffin et al. (2002) with an average crustal composition of  $^{176}\text{Lu}/^{177}\text{Hf} = 0.015$ .

## 4. Results

### 4.1. U-Pb zircon geochronology

A summary of zircon textures and interpretation are shown in Table 2. U-Pb zircon data are presented in supplementary data, concordia diagrams and  $^{207}\text{Pb}/^{206}\text{Pb}$  age spectra are presented in Figs. 3 and 4. Representative cathodoluminescence images of zircons are included in Fig. 5. The samples are subdivided and discussed in accordance to their interpreted protolith.

#### 4.1.1. Igneous lithologies

4.1.1.1. Sample BH12. Sample BH12 is a charnockite composed of K-feldspar + quartz + perthite + plagioclase + antiperthite + orthopyroxene + magnetite + biotite. The rock preserves a strong SW dipping gneissic fabric, defined by biotite, K-feldspar porphyroblasts and magnetite. In sample BH12, 85 spots were ablated on 50 zircons. Weakly luminous cores, rims and well preserved oscillatory zoning were targeted (Fig. 5A). Of the 85 analyses, 79 were between 90 and 110% concordant. A number of older oscillatory zoned cores are interpreted as inherited grains, yielding ages between 1880 and 1700 Ma (Fig. 3A). Weighted averages for weakly luminescent cores, rims and oscillatory zoning yield age estimates of  $1633 \pm 8$  Ma (MSWD = 0.85),  $1639 \pm 9$  Ma (MSWD = 0.72) and  $1639 \pm 8$  Ma (MSWD = 0.83), respectively. As all age estimates fall within error of one another, the best approximation of the crystallisation age is  $1637.8 \pm 4.4$  Ma (MSWD = 1.07), which represents the weighted average age of all analyses.

4.1.1.2. Sample BH15. Sample BH15 is a charnockite that is composed of K-feldspar + quartz + perthite + plagioclase + antiperthite + orthopyroxene + clinopyroxene + magnetite + biotite. The rock preserves a very weak, steeply SW dipping fabric. Seventy-two analyses were obtained from 32 zircons from sample BH15. Luminous rims, oscillatory-zoning and convoluted domains were targeted (Fig. 5B). Of the 72 analyses, 68 were between 90 and 110% concordant. A small

**Table 2**

Description of zircon textures under cathodoluminescence (CL) and the corresponding age estimates of the individual CL domains from across the Ongole Domain.

Sample no.	External zircon morphology	Internal CL textures/features	$^{207}\text{Pb}/^{206}\text{Pb}$ age of CL domains
BH12	100–350 $\mu\text{m}$ ; subhedral to anhedral; prismatic and stubby or ovoid shapes with sub-rounded crystal face terminations; aspect ratios between 2:1 and 6:1.	Two dominant types: 1) Subhedral, dark to weakly luminescent cores surrounded by rims or thick, blurred zoning. 2) Blurred, chaotic oscillatory zoned grains	Weakly luminescent cores: $1633 \pm 8$ Ma Oscillatory zoning: $1639 \pm 8.0$ Ma Luminescent rims: $1639 \pm 9$ Ma
BH15	75 $\mu\text{m}$ – 1.1 mm; prismatic and stubby, or elongate to tabular with sub rounded crystal face terminations. The crystals are largely wholly intact with minimal internal fracturing.	Three dominant zircon types: 1) Blurred and convoluted oscillatory zoned grains 2) Sector zoning preserved around oscillatory zoned or convoluted cores. 3) Dark, mottled cores surrounded by 'ghost zoning'. Cores are partly adsorbed by homogenous weakly luminescent rims or occasionally 'fir tree zoning' within thickened rims surrounding cores.	Convoluted cores: $1637 \pm 9$ Ma Oscillatory zoning: $1633 \pm 8$ Ma Luminescent rims: $1617 \pm 7$ Ma
BH17	30–450 $\mu\text{m}$ ; length to width ratios 2:1 to 4:1; Elongate to tabular in shape with sub-rounded crystal face terminations; A small % of angular fragments and stubby, prismatic grains.	Three dominant types: 1) Approximately half of the zircons are very weakly luminescent and homogenous, with no oscillatory zoning preserved. Blurred and patchy zones of varying luminescence or small, anhedral xenocrystic cores are occasionally preserved. Recognisable rims are rarely developed on these grains. 2) A small number of grains picked in this sample do preserve some oscillatory zoning, either as patches or xenocrystic cores within the crystal; or as zoned rims surrounding convoluted cores. 3) Chaotic, blurred internal textures are extremely common creating multiple domains of varying luminescence within a single crystal.	Homogenous cores: $1578 \pm 16$ Ma Convoluted cores: $1577 \pm 16$ Ma Oscillatory zoning: $1601 \pm 17$ Ma Weakly luminescent rims: $1570 \pm 12$ Ma
BH19	50–200 $\mu\text{m}$ ; variable external morphologies; anhedral to subhedral grains usually prismatic or ovoid in shape; length to width ratios 2:1 to 4:1; sub-rounded to sub-angular crystal face terminations; Many of the grains are angular fragments of larger grains.	The internal morphology of these zircons is extremely chaotic and diverse. 1) Patchy domal zoning, similar to that described by Corfu et al. 2007 is extremely common 2) Homogenous, strongly luminescent grains. 3) Some distorted oscillatory zoning present, but very rare.	Convoluted cores: $1606 \pm 9.4$ Ma Luminescent rims: $1607 \pm 17$ Ma
BH22	150–500 $\mu\text{m}$ ; length to width ratios of between 2:1 and 5:1; Crystal face terminations are sub-rounded to rounded.	Two dominant types: 1) Tabular, elongate zircons are extremely common. The majority of these zircons contain a very strongly luminescent centre which mirrors the same morphology as the external shape of the zircon. 2) Weakly luminescent zircons, often completely homogenous or with patches of chaotic, convoluted sector zoning. A small number of these zircons contain anhedral xenocrystic cores which themselves show oscillatory zoning, or convoluted zoning.	Convoluted cores: $1597 \pm 11$ Ma Luminous cores: $1592 \pm 19$ Ma Weakly luminescent rims: $1598.2 \pm 8.0$
BH08	50–250 $\mu\text{m}$ ; Aspect ratio between 3:1 and 2:1; Predominantly stubby to elongate; Rounded to sub-rounded crystal faces terminations; Small % grains are sub-angular fragments of larger grains.	Subangular elongate or subrounded spherical xenocrystic cores are a common feature in this rock. These cores tend to fit the characteristics of one of three categories; 1) Low luminescence, homogenous cores with sub angular to sub rounded boundaries. 2) Oscillatory zoned or partially zoned elongate to acicular xenocrystic cores. 3) Strongly luminescent convoluted and patchy subrounded to subangular cores.	Large peaks: $1756 \pm 9$ Ma; $1848 \pm 6$ Ma (n = 38, MSWD = 0.46). Smaller peaks: $1643 \pm 15$ Ma; $1958 \pm 12$ Ma; $2149 \pm 21$ Ma; $2255 \pm 16$ Ma; $2319 \pm 14$ ; $2409 \pm 16$ Ma; $2469 \pm 20$ Ma; $2870 \pm 23$ Ma; Youngest detrital grain population: $1723 \pm 21$ Ma
BH16	50–350 $\mu\text{m}$ ; extremely variable external morphologies; elongate to acicular in shape with sub-rounded to sub-angular crystal face terminations; 'tear drop' shaped with sub-rounded to rounded terminations; length to width ratios 3:1 to 5:1.	The external and internal characteristics of these zircon grains were also extremely variable. Grains usually fell into one of three characteristic groups: 1) Oscillatory zoned xenocrystic cores. Zoning is usually convoluted or thickened. Thin ( $<10$ $\mu\text{m}$ ) to thick rims ( $20$ – $40$ $\mu\text{m}$ ) are commonly bound these cores. 2) Weakly luminescent homogenous grains with no distinguishable core or rim. 3) Euhedral, broken fragments which feature chaotic internal textures and are largely fractured and metamict. Highly variable internal luminescence within sector zoning or relic oscillatory zoning.	Large peaks: $1652.6 \pm 4.2$ Ma; $1728 \pm 5.8$ Ma Smaller peaks: $1576 \pm 22$ Ma; $1836 \pm 22$ Ma; $2003 \pm 19$ Ma; $2103 \pm 18$ Ma. $2320 \pm 24$ Ma; $2434 \pm 24$ Ma Youngest detrital grain population: $1709 \pm 19$ Ma
I0508	50 and 300 $\mu\text{m}$ ; Length to width ratios 2:1 and 4:1; Sub-rounded to rounded crystal face terminations. Elongate to prismatic; Often metamict and corroded along some boundaries, resulting in irregular and abstract shapes; Smaller, ovoid grains are also frequent.	1) Oscillatory zoned cores, partially recrystallised resulting in thickened, blurred domains (Reference) 2) Homogenous, xenocrystic cores. Homogenous cores are either strongly luminescent or very weakly luminescent. Strongly luminescent cores are occasionally surrounded by weakly luminescent, thin ( $\sim 20$ $\mu\text{m}$ ) rims. In these grains fracturing often propagates from the cores outwards to the rims. This could be interpreted as expansion within the luminescent, U rich domains resulting in cracking and fracturing into the adjacent, more brittle U poor domains	Large broad peaks: $1593.7 \pm 20$ Ma, $1626.3 \pm 14$ Ma $1666 \pm 18$ Ma Smaller peaks: $1781 \pm 26$ Ma; $2140 \pm 25$ Ma; $2330 \pm 15$ Ma; $2416 \pm 17$ Ma; $2488 \pm 24$ Ma; $2573 \pm 18$ Ma; $2636 \pm 23$ Ma; $2769 \pm 17$ Ma Youngest detrital grain population: $1718 \pm 18$ Ma

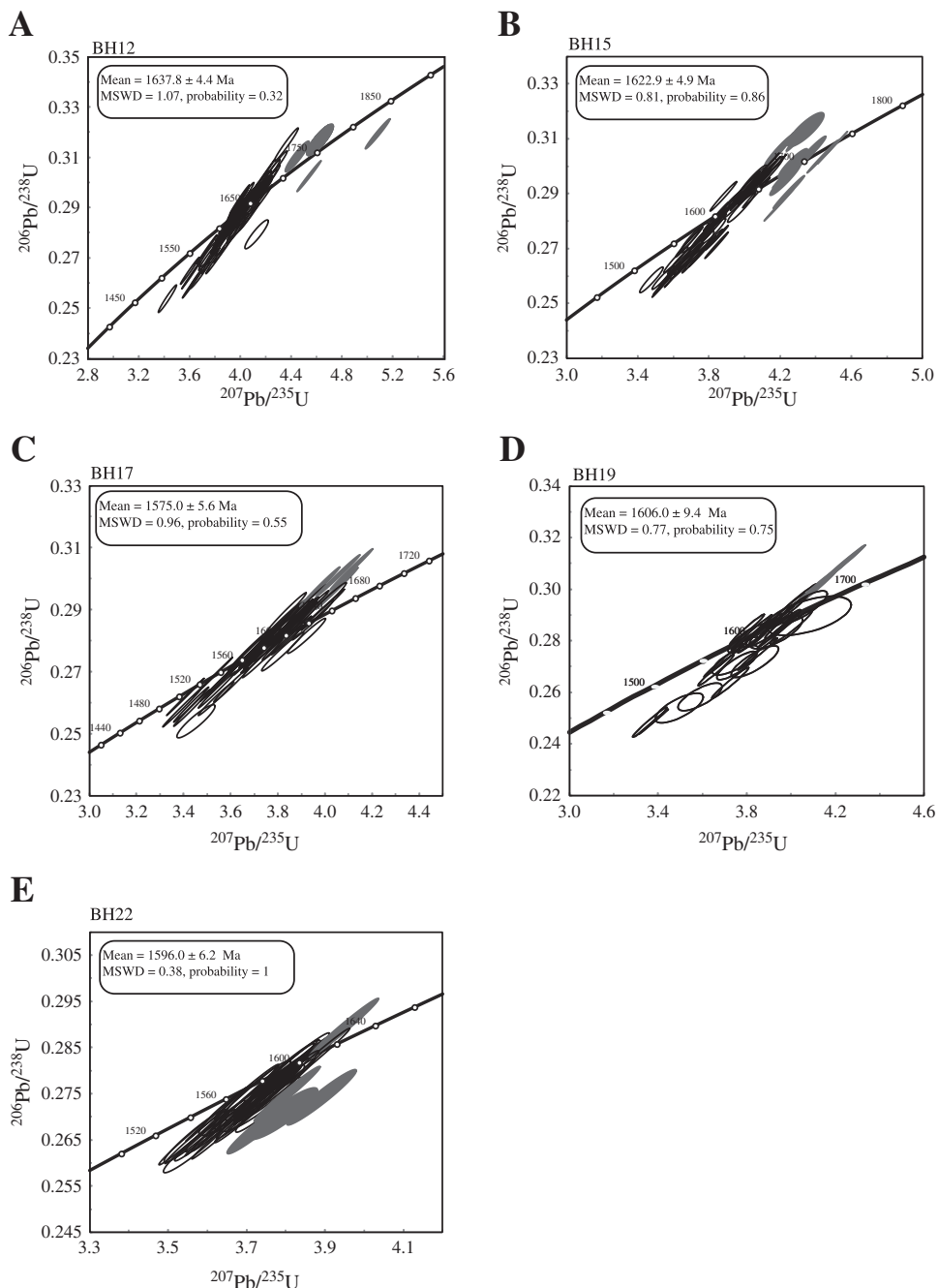


**Fig. 3.** Concordia plots for zircon grains from igneous rock samples from the Ongole Domain. Mean ages displayed are  $^{207}\text{Pb}/^{206}\text{Pb}$  ages with mean errors quoted at the one standard deviation level. Solid grey ellipses represent inherited zircon grains.

number of cores are interpreted as inherited, yielding ages between 1740 and 1700 Ma (Fig. 3B). A weighted average  $^{207}\text{Pb}/^{206}\text{Pb}$  age of the oscillatory-zoned cores produced an age estimate of  $1633 \pm 8$  Ma (MSWD = 1.2) and convoluted cores yield a weighted mean of  $1637 \pm 9$  Ma (MSWD = 1.5). Strongly luminescent rims generate a younger  $^{207}\text{Pb}/^{206}\text{Pb}$  weighted mean of  $1617 \pm 7$  Ma (MSWD = 0.77). As the rim analyses yield an age outside of uncertainty of the ages obtained from the zircon cores the two ages are interpreted to be distinct zircon growth events. Oscillatory-zoned cores are interpreted to represent crystallisation of the magmatic protolith.

**4.1.1.3. Sample BH17.** BH17 is a charnockite composed of K-feldspar + quartz + perthite + plagioclase + orthopyroxene + clinopyroxene + magnetite + biotite. The rock is unfoliated. Fifty-four spots were

analysed on 40 zircon grains from sample BH17, which targeted four specific CL domains. These are: homogenous weakly luminescent cores, weakly luminescent rims, patchy or convoluted cores, and well-preserved oscillatory-zoning (Fig. 5C). All grains analysed were 90–110% concordant. Collectively, all concordant data generate a weighted average age estimate of  $1575 \pm 5.6$  Ma with an MSWD of 0.96. The ages of homogenous and convoluted cores are inseparable and yield average ages of  $1577 \pm 16$  Ma (MSWD = 2.1) and  $1578 \pm 10$  Ma (MSWD = 0.93). Weakly luminescent rims yield a slightly younger weighted average age of  $1570 \pm 12$  Ma (MSWD = 0.73), albeit within analytical uncertainty. Oscillatory-zoned domains generate a weighted average of  $1601 \pm 17$  Ma (MSWD = 0.47). A small number of oscillatory-zoned cores are interpreted to have been inherited, yielding ages between 1705 and 1675 Ma (Fig. 3C). Although

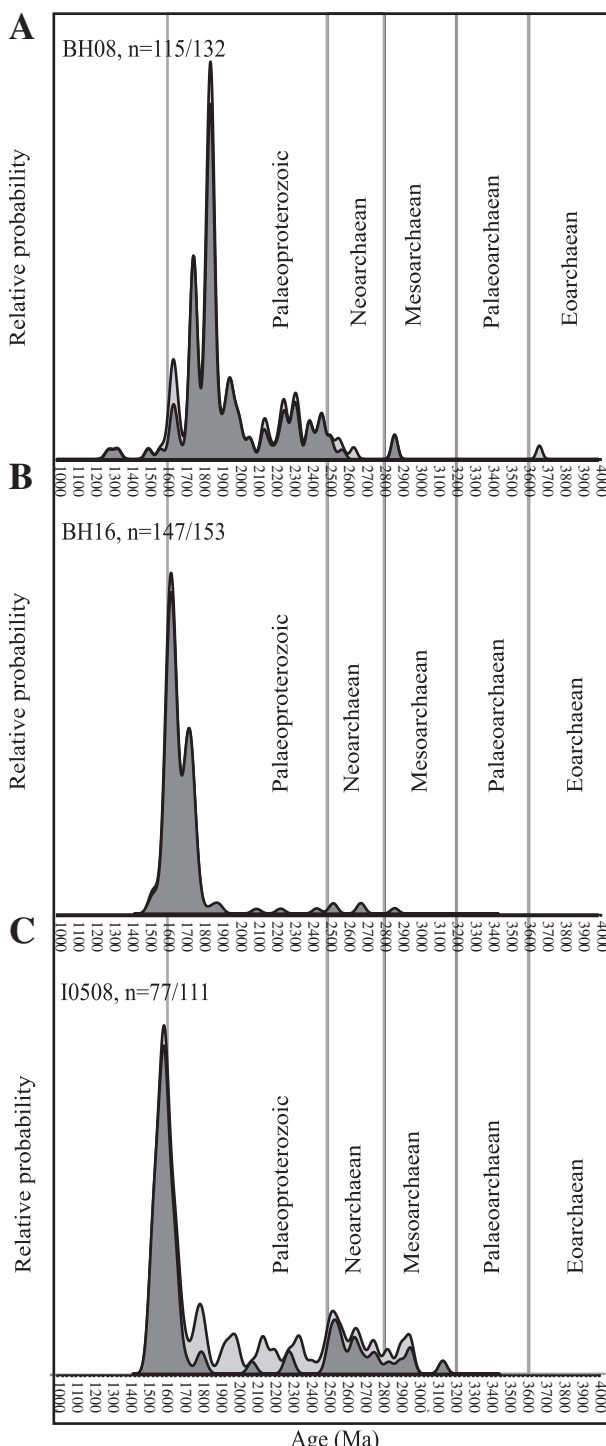


**Fig. 4.** Detrital zircon age probability density distributions from the Ongole Domain metasedimentary rocks. Lighter grey fields represent zircon grains that are >10% discordant.  $n = \text{xxx}/\text{xxx}$  equals number of >90–110% concordant analyses/number of <90% or >110% concordant analyses.

there is some variation in the targeted domains, with the oldest ages being from the cores and the younger from the rims, the imprecision of the LA-ICPMS technique means that all results fall within error of one another and the collective weighted average age is considered the most accurate approximation of crystallisation.

**4.1.1.4. Sample BH19.** Sample 19 is a medium grained, homogenous granite composed of quartz + plagioclase + perthite + biotite. Fifty

six analyses were obtained on 47 zircon grains from sample BH19. Ablation targeted patchy, convoluted zoning in cores and strongly luminescent rims (Fig. 5D). Twenty eight of the 56 results were between 90 and 110% concordant (Fig. 3D). A small number of concordant grains are aged between 1670 and 1650 Ma, and are interpreted to be inherited. A weighted average of the remaining concordant data produces an age of  $1606 \pm 9.4$  Ma (MSWD = 0.77). Analyses from strongly luminescent rims yield a weighted average age of  $1607 \pm 17$  Ma (MSWD = 0.051). The CL domains are statistically indistinguishable and thus the weighted average of all samples is the most reliable representation of the zircon crystallisation.

**4.1.1.5. Sample BH22.** Sample BH22 is a quartz monzonite composed of quartz + perthite + plagioclase + biotite + hornblende. It is undeformed but contains a pervasive network of isoclinally folded quartz leucosomes. Fifty six spots were ablated on 47 zircon grains from sample BH22, targeting homogenous and xenocrystic cores, strongly luminescent domains and weakly luminescent rims (Fig. 5E). Forty seven of 54 analyses were between 90 and 110% concordant. Collectively, all analyses yield a weighted average age estimate of  $1596 \pm 6.2$  Ma (MSWD = 0.38). All individual domains are statistically identical to the cumulative weighted average generating age estimates of  $1597 \pm 11$  Ma,  $1592 \pm 19$  Ma and  $1598 \pm 8$  Ma for homogenous cores (MSWD = 0.52), luminescent domains (MSWD = 0.18), and weakly luminescent rims (MSWD = 0.47) respectively. A small number of grains are interpreted as inherited yielding ages between ca. 1680 and 1640 Ma. The domains are statistically indistinguishable and thus the weighted average of all analyses is considered the most reliable representation of the zircon crystallisation age.

#### 4.1.2. Metasedimentary rocks

**4.1.2.1. Sample BH08.** Sample BH08 is a garnet–sillimanite–cordierite metapelite that preserves a strong, steeply dipping, NW fabric and isoclinal folding. 132 spots were ablated on 71 grains. Oscillatory-zoning, homogenous cores, rims and convoluted cores were targeted (Fig. 5F). The dominant populations evident in this sample are  $1756 \pm 9$  Ma ( $n = 21$ , MSWD = 0.33) and  $1848 \pm 6$  Ma ( $n = 38$ , MSWD = 0.46). Smaller peaks also occur at ca. 2870, 2470, 2410, 2320, 2260, 2150, 1960, and 1640 Ma (Fig. 4A). The 1640 Ma population occurs exclusively as rims on older grains, or as low luminescence, rounded grains typical of metamorphic origin. On this basis, the ca. 1640 Ma age population is interpreted as metamorphic. The youngest interpreted detrital grain is  $1723 \pm 20$  Ma.

**4.1.2.2. Sample BH16.** Sample BH16 is an OPX-garnet bearing metapelite that preserves a moderate N-S trending fabric. 153 analyses were conducted on 81 zircon grains targeting four CL domains; convoluted and patchy cores, oscillatory zoning, weakly homogenous cores and rims (Fig. 5G). A large, bimodal, concordant distribution exists with peaks at ca. 1680–1620 Ma ( $n = 87$ ) and ca. 1760–1710 Ma ( $n = 46$ ). Concordant data from these peaks yield weighted average age estimates of  $1652 \pm 4$  Ma (MSWD = 0.51) and  $1728 \pm 6$  Ma (MSWD = 0.27) respectively. The younger peak is interpreted to date the growth of metamorphic zircon. Zircon grains from this population are typically featureless, or exhibit heavily blurred patchy zoning (Fig. 5G). A number of analyses from this population are rims on older grains. Smaller peaks occur at ca. 2430, 2320 and 1840 Ma (Fig. 4B), and singular concordant zircon grains also yield ages of  $2003 \pm 19$  Ma and  $2103 \pm 18$  Ma. The youngest interpreted detrital zircon grain forms part of the 1728 Ma population, yielding an age of  $1709 \pm 19$  Ma.

**4.1.2.3. Sample I0508.** Sample I0508 is a quartzite composed of quartz + perthite + sillimanite + ilmenite. In sample I0508, 104 analyses were conducted on 72 zircons. Convolute cores, homogenous cores, oscillatory zoning and rims were targeted (Fig. 5H). The main population of

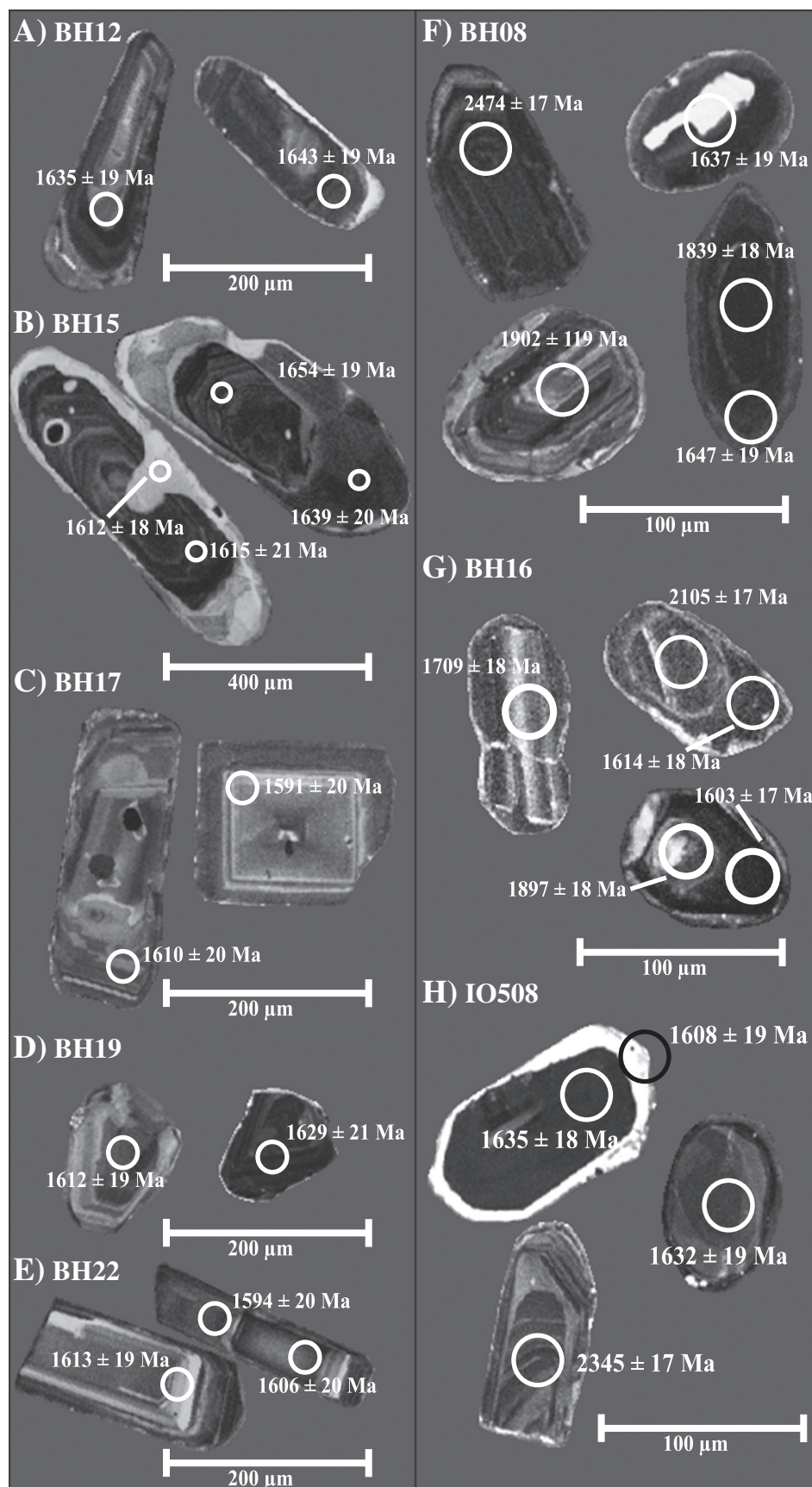


**Fig. 5.** CL images of representative zircon grains from the Ongole Domain, (A) Zr10 and Zr21 of sample BH12, (B) Zr25 and Zr26, Zr43 and Zr44 of sample BH15, (C) Zr29 and Zr42 of sample BH17, (D) Zr50 and Zr39 of sample BH19, (E) Zr38, Zr28 and Zr29 of sample BH22, (F) Zr107, Zr79, Zr120, Zr69 and Zr70 from sample BH08, (G) Zr16, Zr57 and Zr58, Zr24 and Zr25, (H) Zr41 and Zr42, Zr25, and Zr86 from sample IO508.

zircon grains occurs in a broad peak from ca. 1680 to 1590 Ma ( $n = 49$ ) with a weighted average age estimate of  $1625 \pm 8$  Ma (MSWD = 2.4). Zircon grains from this population exhibit characteristics typical of grains modified by metamorphism. Grains preserve sector zoning, blurred zoning, or are generally featureless (Fig. 5H). The broad smear of ages between ca. 1680 and 1590 Ma is interpreted here as isotopic re-setting and/or continual growth of zircon as a result of metamorphism. Smaller peaks yield ages of ca. 2640, 2570, 2490, 2420, 2330, 2140, 1780 and 1730 Ma and one singular zircon yields an age of  $2769 \pm 17$  Ma (Fig. 4C). The youngest interpreted detrital zircon grain forms part of the small 1730 Ma peak, yielding a single age of  $1718 \pm 18$  Ma. The ca. 1730 Ma peak is interpreted to represent the youngest detrital population in this sample.

#### 4.2. Monazite geochronology results

##### 4.2.1. BH09

Sample BH09 is a garnet–sillimanite–cordierite bearing metapelite that preserves a strong, steeply dipping NW fabric and isoclinal folding. 28 in-situ analyses were conducted on 28 monazite grains in sample BH09. 19 grains were <5% discordant, with the bulk of the concordant monazites located within garnet grains ( $n = 14$ ). The remainder were located in sillimanite ( $n = 4$ ) and cordierite grains ( $n = 1$ ) that formed the matrix of the rock. Monazite grains are typically 20–50  $\mu\text{m}$  in size and are subhedral to euhedral in shape (Fig. 6A).

A weighted average of all concordant (95–105%) data yields a  $^{206}\text{Pb}/^{207}\text{Pb}$  age estimate of  $1588 \pm 11$  Ma (Fig. 6A, MSWD = 0.22).

A single grain located within cordierite yielded the youngest concordant age of  $1475 \pm 29$  Ma, and was not included in the calculation of the weighted average. When the data is separated in accordance with the textural location of the monazite, grains residing within garnets yield weighted average age estimates of  $1588 \pm 12$  Ma (MSWD 0.26) and grains located within the matrix sillimanite yield age estimates of  $1590 \pm 24$  Ma (MSWD = 0.106).

##### 4.2.2. BH16

Thirty four in-situ analyses of 30 monazite grains were performed on sample BH16. Of these, 20 grains were <5% discordant. Just over half of the grains ablated were located within euhedral porphyroblasts of garnet ( $n = 12$ ), with the remainder of grains found within matrix ilmenite ( $n = 5$ ), quartz ( $n = 1$ ), K-feldspar ( $n = 1$ ) and biotite ( $n = 1$ ). Monazites are between 30 and 100  $\mu\text{m}$  in size and are usually subhedral to euhedral in garnets or cuspatate, irregular grains within the matrix of the rock (Fig. 6B). BSE imaging reveals that there is very little chemical variation in the monazites.

A concordia of all concordant (95–105%) data reveal a population at ca. 1600 Ma and a small number of grains between ca. 1680–1640 Ma. A weighted average age estimate of all the grains yields a  $^{206}\text{Pb}/^{207}\text{Pb}$  age of  $1607 \pm 17$  Ma (MSWD = 2.9). When the small population of older outliers is removed from the estimate ( $n = 4$ ), the average is  $1593 \pm 10$  Ma (Fig. 6B, MSWD = 1.08). When the data are separated in accordance to the textural location of the monazites, grains hosted within garnet yield the oldest population of monazites (ca. 1684–1640 Ma), as well as a concordant population between

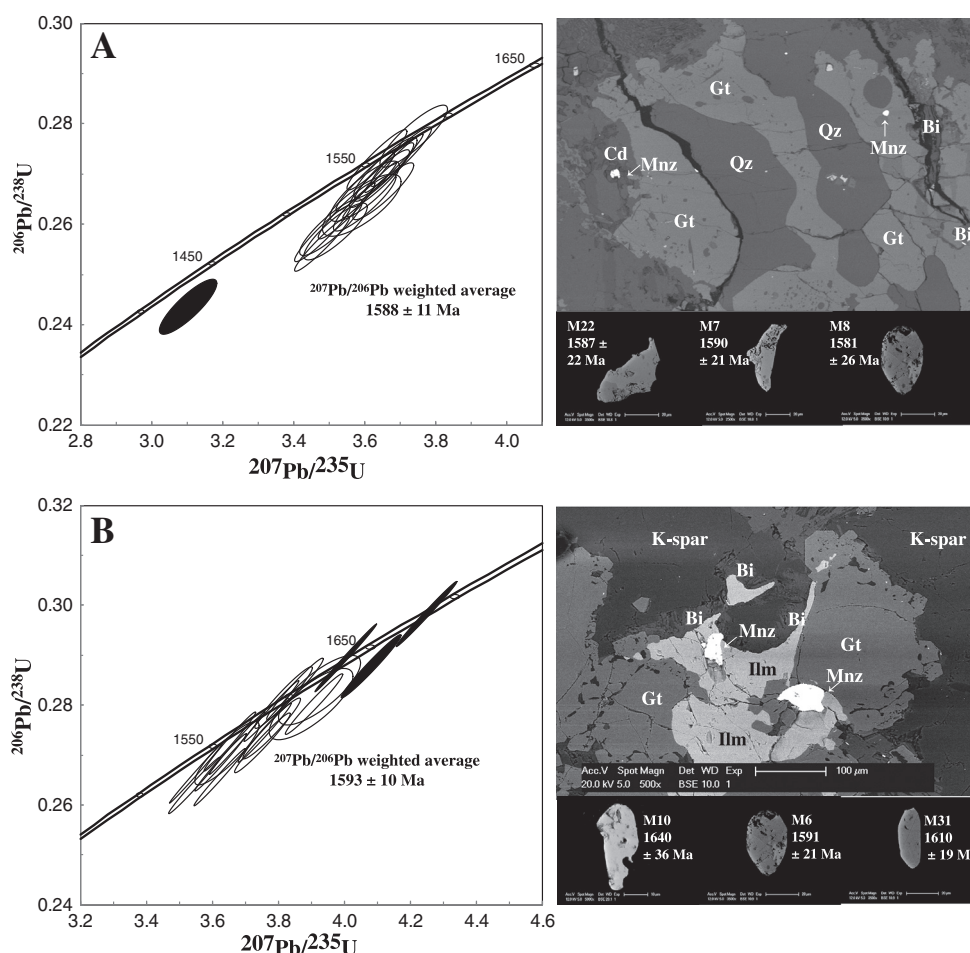


**Fig. 6.** Concordia plots (left) of 95–105% concordant monazite data from A) sample BH09 and B) sample BH16, and backscattered electron images (BSE) of in-situ and isolated monazite grains (right). Solid ellipses are outliers and were not included in the mean weighted average of the monazite grains. Magnified BSE images of individual grains (lower left) are shown to emphasise the texture and morphology of the monazite grains analysed.

1630 and 1548 Ma. The remainder of the monazite grains found within matrix minerals yield a weighted average age of  $1593 \pm 15$  Ma (MSWD = 0.92).

#### 4.3. Zircon Lu-Hf results

Zircon Lu-Hf isotope results are provided in supplementary data and displayed in Figs. 7 and 8. Data were obtained from three metasedimentary rock samples; BH08, BH16 and I0508; and from five meta-igneous samples; BH12, BH15, BH17, BH19 and BH22.

Representative grains were chosen from peak U-Pb age populations at ca. 2860, 2760, 2640, 2510, 2400, 2310, 2245, 2140, 2100, 1950, 1850, 1745, 1640 Ma in samples BH08, BH16 and I0508. Present-day Hf isotopic compositions range from 0.280898 to 0.281757 for the grains, corresponding to predominantly evolved epsilon hafnium ( $\epsilon_{\text{Hf}(T)}$ ) values that range from -18 to +7 (Fig. 7). Crustal model ages ( $T_{\text{DMc}}$ ) were calculated for each zircon assuming average continental crust with  $^{176}\text{Lu}/^{177}\text{Hf}$  values of 0.0015 (Griffin et al., 2008) as the zircon grain growth reservoir. Based on this crustal model, a broad age range of ca. 3.5–2.3 Ga  $T_{\text{DMc}}$  is obtained for the detrital zircon grains. Broad similarities between the detrital zircon-age spectra across the three metasedimentary samples suggest similar sources were involved in the derivation of the sedimentary protolith rocks; therefore the Lu-Hf isotope results are discussed by U-Pb age populations, rather than by sample.

The  $\epsilon_{\text{Hf}(T)}$  values are variable within the detrital zircon peaks identified in the metasedimentary rocks from the Ongole Domain, but are predominantly evolved. The oldest zircon grains analysed have  $^{207}\text{Pb}/^{206}\text{Pb}$  crystallisation ages of ca. 2769 and ca. 2868 Ma, and yield  $\epsilon_{\text{Hf}(T)}$  values of -5 and -1 ( $T_{\text{DMc}}$  of 3.4 and 3.5 Ga, respectively). A single 2635 Ma grain yields an  $\epsilon_{\text{Hf}(T)}$  value of -2 ( $T_{\text{DMc}}$  of 3.3 Ga). Two grains aged 2589 and 2547 Ma yield  $\epsilon_{\text{Hf}(T)}$  values of -6 and -3, respectively ( $T_{\text{DMc}}$  of 3.4 and 3.2 Ga). A single 2516 Ma grain yields a positive  $\epsilon_{\text{Hf}(T)}$  value of +4 and a corresponding  $T_{\text{DMc}}$  of 2.8 Ga. Zircon grains aged between ca. 2400–2440 Ma record variable  $\epsilon_{\text{Hf}(T)}$  values between -9 and 0 ( $T_{\text{DMc}}$  of 3.4–3 Ga). Detrital zircon grains aged between 2350 and 2280 Ma also yield variable  $\epsilon_{\text{Hf}(T)}$  values between -12 and -1 ( $T_{\text{DMc}}$  of 3.6–2.9 Ga). A population of grains between 2250 and 2100 Ma yield highly variable  $\epsilon_{\text{Hf}(T)}$  values between -18 and +7, and corresponding  $T_{\text{DMc}}$  of 3.8–2.3 Ga. Detrital zircon grains between 2000 and 1950 Ma yield near chondritic  $\epsilon_{\text{Hf}(T)}$  values between -2 and 0 ( $T_{\text{DMc}}$  of 2.7–2.6 Ga). Grains from the age range ca. 1850–1600 Ma all yield  $\epsilon_{\text{Hf}(T)}$  values between -10 and -1 ( $T_{\text{DMc}}$  of 2.9–2.4 Ga).

Igneous zircon grains yield U-Pb ages between ca. 1660 and 1580 Ma and present day Hf isotopic compositions of 0.281417 to 0.281684.

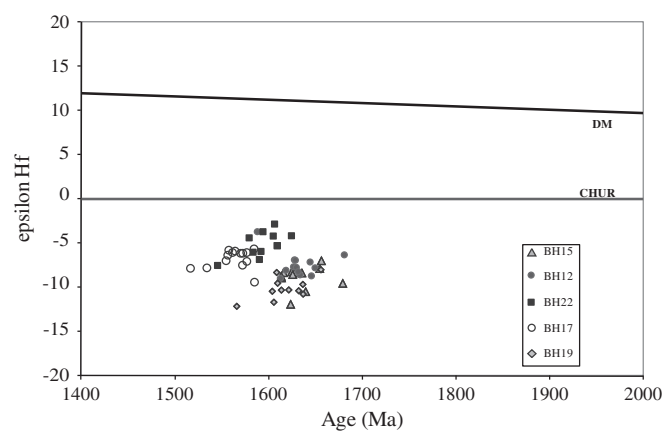


Fig. 8.  $\epsilon_{\text{Hf}}$  values plotted against  $^{207}\text{Pb}/^{206}\text{Pb}$  ages for individual zircon grains from five igneous samples from Area 1B in the Ongole Domain (BH12, BH15, BH17, BH19 and BH22).

Corresponding  $\epsilon_{\text{Hf}(T)}$  values range from -12 to -2, and  $T_{\text{DMc}}$  varied between 2.5 and 3 Ga (Fig. 8).

Zircon grains analysed from sample BH12 (mean = 1635 Ma) yield consistent  $\epsilon_{\text{Hf}(T)}$  values -6 to -8 ( $T_{\text{DMc}}$  2.7–2.8 Ga). Grains from sample BH15 yield similar U-Pb ages (mean = 1630 Ma) record predominantly evolved  $\epsilon_{\text{Hf}(T)}$  values between -11 and -7 ( $T_{\text{DMc}}$  2.8–3 Ga). Zircon grains from sample BH17 are comparatively younger (mean = 1560 Ma), yielding  $\epsilon_{\text{Hf}(T)}$  values between -7 and -5 ( $T_{\text{DMc}}$  2.6–2.7 Ga). Grains analysed from sample BH19 (mean = 1610 Ma) are evolved yielding  $\epsilon_{\text{Hf}(T)}$  values between -11 and -8 ( $T_{\text{DMc}}$  2.8–3 Ga). Grains analysed from sample BH22 (mean = 1595 Ma) yield  $\epsilon_{\text{Hf}(T)}$  values between -6 and -3 ( $T_{\text{DMc}}$  2.5–2.6 Ga).

## 5. Discussion

### 5.1. Depositional age and provenance of the metasedimentary protolith rocks

Granulite-facies metamorphism and deformation in the Ongole Domain mean that primary sedimentary features are destroyed, and the paucity of outcrop means there is no direct evidence linking the sampled metasedimentary rocks to the same sedimentary succession. All three samples record a small percentage of Mesoarchaean–Neoarchaean detritus, and variable percentages of Palaeoproterozoic detritus. Sample BH08 records two significant late Palaeoproterozoic populations (ca. 1850 and 1750 Ma), by comparison to samples BH16 and I0508. However, broad similarities in detrital zircon-age spectra across the three samples suggest similar source regions were involved in the formation of the sedimentary protoliths.

High-grade metamorphism is interpreted to have affected the zircons preserved in the Ongole Domain metasedimentary rocks, with metamorphic zircon recognised between ca. 1680 and 1590 Ma (present study). The maximum age of deposition is interpreted as ca. 1720 Ma, which represents the youngest detrital population. An earlier metamorphic event has been proposed to have occurred in the Ongole Domain at ca. 1760 Ma (Bose et al., 2011). However the presence of detrital grains within the metasedimentary rocks as young as ca. 1718 Ma weakens the evidence for this event.

Prevailing continental reconstructions of Columbia attempt to constrain the location of India, and by default the Krishna Province, during the Palaeoproterozoic and Mesoproterozoic. The time at which Columbia amalgamated is contested, but is generally considered to have occurred between ca. 2100–1800 Ma (Zhao et al., 2004; Hou et al., 2008; Evans and Mitchell, 2011), and subsequently broke apart during rifting over a long period between 1700 and 1300 Ma (Ernst et al., 2008; Evans and Mitchell, 2011). Recent reconstruction models place proto-India in three discrete geographic locations: 1) juxtaposed against the Napier

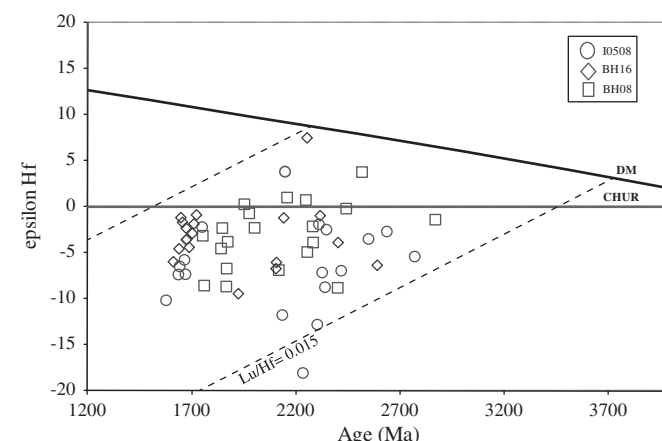


Fig. 7.  $\epsilon_{\text{Hf}}$  values plotted against  $^{207}\text{Pb}/^{206}\text{Pb}$  ages for individual zircon grains from three metasedimentary samples from Area 1A in the Ongole Domain (BH08) and Area 1B in the Ongole Domain (BH16 and I0508). The continental evolution lines were calculated by using  $^{176}\text{Lu}/^{177}\text{Hf} = 0.015$  (Griffin et al., 2002).

Complex (NC), East Antarctica (EA) and the North China Craton (NCC) (Zhao et al., 2002; Zhao et al., 2004) at ca. 1.85 Ga; 2) adjacent to the North Australian Craton (NAC) and Gawler Craton (GC) at ca. 1.59 Ga (Zhang et al., 2012) and 3) adjacent to the NCC at ca. 1.85 Ga (Hou et al., 2008). These terranes are investigated as potential source terranes for the Ongole Domain metasedimentary protolith rocks. As the Archaean eastern Dharwar Craton has been previously considered as the dominant source for the Ongole Domain metasedimentary rocks (Rickers et al., 2001), this terrane is also considered for provenance.

Mesoarchaean to Palaeoproterozoic source terranes are required to account for the broad range of detrital peaks between ca. 2900–1850 Ma. A compilation of the major zircon forming events in the NC, NCC, DC, NAC and the GC are contrasted against the Ongole Domain detrital signature in Fig. 9. What is evident is that although these terranes fit one or a number of the detrital peaks seen in the Ongole Domain metasedimentary rocks, the overall best fit is the NAC, and to a lesser extent the GC. Palaeoproterozoic metasedimentary sequences in the Tanami region and Aileron Province of the NAC are dominated by major detrital zircon populations of ca. 1880–1830 Ma and ca. 1780–1730 Ma (Cross and Crispe, 2007; Claoué-Long et al., 2008a), which is very similar to the primary populations in the Ongole Domain metasedimentary rocks. Additionally, the Palaeoproterozoic sequences from the NAC contain subordinate detrital populations up to ca. 2900 Ma (Cross and Crispe, 2007; Claoué-Long et al., 2008a), which closely match the Ongole Domain detrital populations at ca. 2650–2600, 2460, 2320, 2260, 2200–2100, 2080–2010 and 1980–1920 Ma (Fig. 9). This suggests that the source of these NAC detrital zircons is similar to that of the Ongole Domain protoliths. As rocks older than the Neoarchaean have not been recognised in the NAC, it seems unlikely that the NAC is the direct source for Ongole Domain metasedimentary protoliths but does raise the possibility that they were in the proximity of the same source terrane(s).

The Napier Complex is also a good fit for a number of Palaeoproterozoic to Neoarchaean peaks (ca. 2880, 2770, 2640, 2600, 2550–2450, 2350, 2250 Ma), but records only minor zircon generation between 2100 and 1750 Ma (Fig. 9). Hokada et al. (2003) report 2850–2790 Ma zircon grains at Mt Riiser-Larsen; which, on the basis of zircon CL characteristics, they have interpreted to reflect a high temperature metamorphic event associated magmatism at ca. 2830 Ma. Horie et al. (2012) report detrital zircon grains for quartzo-feldspathic gneisses and quartzites from Mt. Cronus and Fyfe Hills between 3218 and 2550 Ma, overlapping with a number of populations seen in the Ongole Domain metasedimentary protoliths (ca. 2880, 2770, 2640, 2550 Ma). Early Paleoproterozoic zircon (2492–2490 Ma) are documented by Horie et al. (2012) broadly coinciding with UHT metamorphism in the Napier Complex proposed to have occurred between 2550 and 2480 Ma (Carson et al., 2002). Younger zircon grains/domains from Fyfe Hills/Mt. Cronus were also reported between ca. 2400 and ca. 1800 Ma, with significant populations at ca. 2380, 2200 and 1820 Ma. Previous authors have also reported similar ages from the Napier Complex (Grew et al., 2001; Carson et al., 2002; Owada et al., 2001; Suzuki et al., 2006).

The Precambrian evolution of the NCC is related to three major events at ca. 2700, 2500 and 2000–1820 Ma (Zhai and Santosh, 2011). The NCC is dominated by a ca. 2700 Ma magmatic zircon U–Pb age population, related to voluminous tonalite–trondhjemite–granodiorite

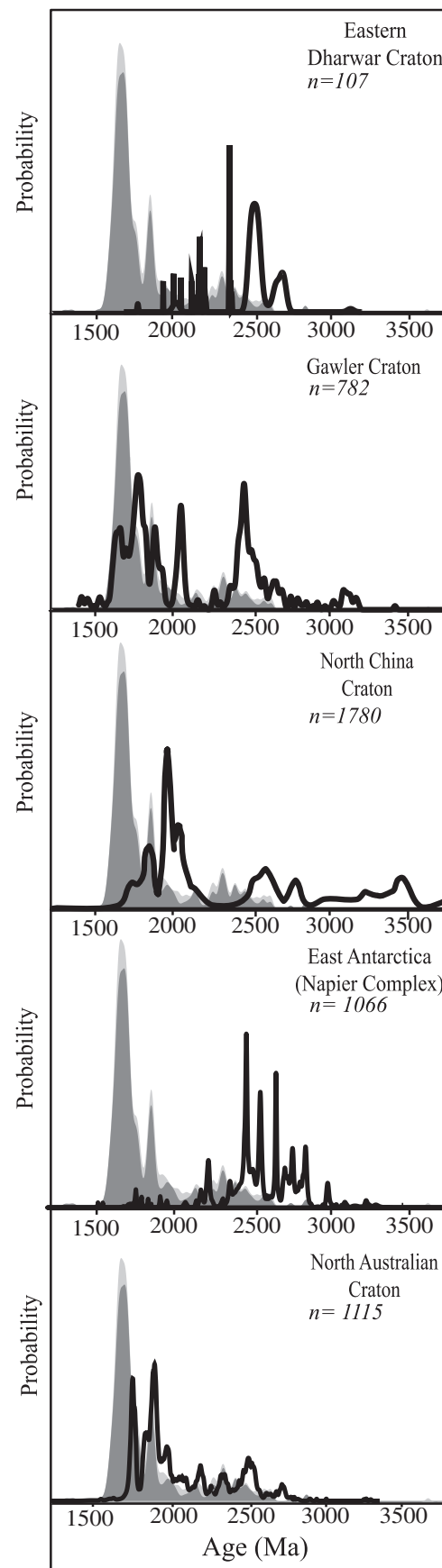


**Fig. 9.** Combined probability density plots for all zircon grains from the metasedimentary rocks from the Ongole Domain (represented by the solid grey fields) shown in comparison to the major zircon forming events of the Dharwar Craton, Gawler Craton, North China Craton, East Antarctica (Napier Complex) and the North Australian Craton. N = number of analyses included in the comparison. Zircon data for comparative regions is compiled from Lanyon et al. (1993), Zhao and Bennett (1995), Jayananda et al. (2000), Carson et al. (2002), Guan et al. (2002), Hokada et al. (2003), Jayananda et al. (2006), French and Heaman (2010), Swain et al. (2005), Suzuki et al. (2006), Wang et al. (2007), Claoué-Long et al. (2008a, 2008b), Belousova et al. (2009), Liu et al. (2009), Horie et al. (2011), Yin et al. (2011), Zhai and Santosh (2011) and Guitreau et al. (2012).

(TTG) generation and crustal growth (Guan et al., 2002; Liu et al., 2009). The amalgamation of microcontinental blocks at ca. 2500 Ma (Zhai et al., 2010) to form a stable craton, was associated with the generation of granitoids that yield U-Pb zircon ages between ca. 2530–2450 Ma (Guan et al., 2002; Kröner et al., 2005; Zhang et al., 2006).

Only a minor percentage of detrital grains from the Ongole Domain are Neoarchaean or older, suggesting it is unlikely a large percentage of detritus was inherited from the Archaean NCC terranes. A period of rifting and extension affected the NCC between ca. 2300–2000 Ma (Zhai and Santosh, 2011), and was followed by HP-UHT metamorphism between 1950 and 1820 Ma (Santosh et al., 2006). Zircon grains generated in the NCC during the mid-late Palaeoproterozoic do overlap with peak detrital populations (ca. 1850, 1980–1920 Ma) in the Ongole Domain (Fig. 9).

The eastern Dharwar Craton is also characterised by voluminous magmatism between ca. 2700 and 2500 Ma (Jayananda et al., 2000), a peak which is noticeably small in the Ongole Domain detrital zircons. A number of other important detrital populations are missing in the DC (ca. 2450–2400, 2350, 2250, 1850 Ma, Fig. 9), suggesting it is unlikely that the protolith sedimentary rocks were sourced directly from the eastern Dharwar Craton.

Zircon hafnium isotopes further test the hypothesised matches between the Ongole Domain detrital zircon age populations and possible source terranes. An immediate issue recognised by this study is the lack of comparative hafnium isotopes from the Dharwar Craton and East Antarctica. However, it is possible to tentatively appraise the hafnium isotope characteristics of the Ongole Domain detrital zircons, against those reported for the NAC, GC, and the NCC (Fig. 10A–C). With the exception of five grains between 2500 and 2200 Ma, the Ongole Domain detrital zircons all exhibit  $\epsilon_{\text{Hf}(T)}$  values close to, or below, CHUR (average  $\epsilon_{\text{Hf}(T)} = -4$ ). This indicates that the reworking of Mesoarchaean crust played a significant role in the generation of the Palaeoproterozoic–Archaean detrital zircons. Some similarities exist between the Hf isotopic populations of the Ongole Domain and the NAC, GC and NCC. The ca. 1850 Ma detrital peak seen in the Ongole Domain metasedimentary rocks falls within the broad isotopic range of zircons generated with the GC during this period (Belousova et al., 2009). There is a small overlap with ca. 1850 Ma zircons recorded in the NAC (Claué-Long et al., 2008b) and with the NCC (Yin et al., 2011). Similarly, a broad overlap between the Ongole Domain and GC zircons at ca. 2400 Ma, where the GC records zircon production related to the Sleafordian Orogeny (Hand et al., 2007; McGee et al., 2010). However, the majority of the late Archaean–Palaeoproterozoic zircons generated in the GC, NAC and NCC terranes are more juvenile than those recorded in the Ongole Domain (Fig. 10A–B). Interestingly, the Palaeoproterozoic zircon grains from the NCC are isotopically very similar to those of the NAC (Fig. 10B–C).

The linear expansion of  $\epsilon_{\text{Hf}(T)}$  values at ca. 2200 Ma in the Ongole Domain suggests derivation from a terrane that underwent reworking during this period (Kemp et al., 2006). An event of this age is not recognised in the GC, NAC or NCC. In the Napier Complex, a ca. 2250–2200 Ma thermal event associated with deformation, metamorphism and pegmatite emplacement has been interpreted in both monazite, xenotime and zircon data (Grew et al., 2001; Asami et al., 2002; Horie et al., 2012); but very little is understood regarding the extent and characteristics of this event.

The geochronological and isotopic data suggest that the Ongole Domain sedimentary protolith rocks were not derived from the Dharwar Craton, but were deposited on another terrane that was later accreted to proto-India. The most appropriate candidate is the Napier Complex of East Antarctica, which lay next to the Ongole Domain in Gondwana (e.g. Collins and Pisarevsky, 2005). No candidate Proterozoic suture between the Napier Complex and the Ongole Domain that could have brought the two together has yet been recognised. In addition, the geochronological similarities between events recorded in the Napier Complex and the Ongole Domain protolith sedimentary rocks make

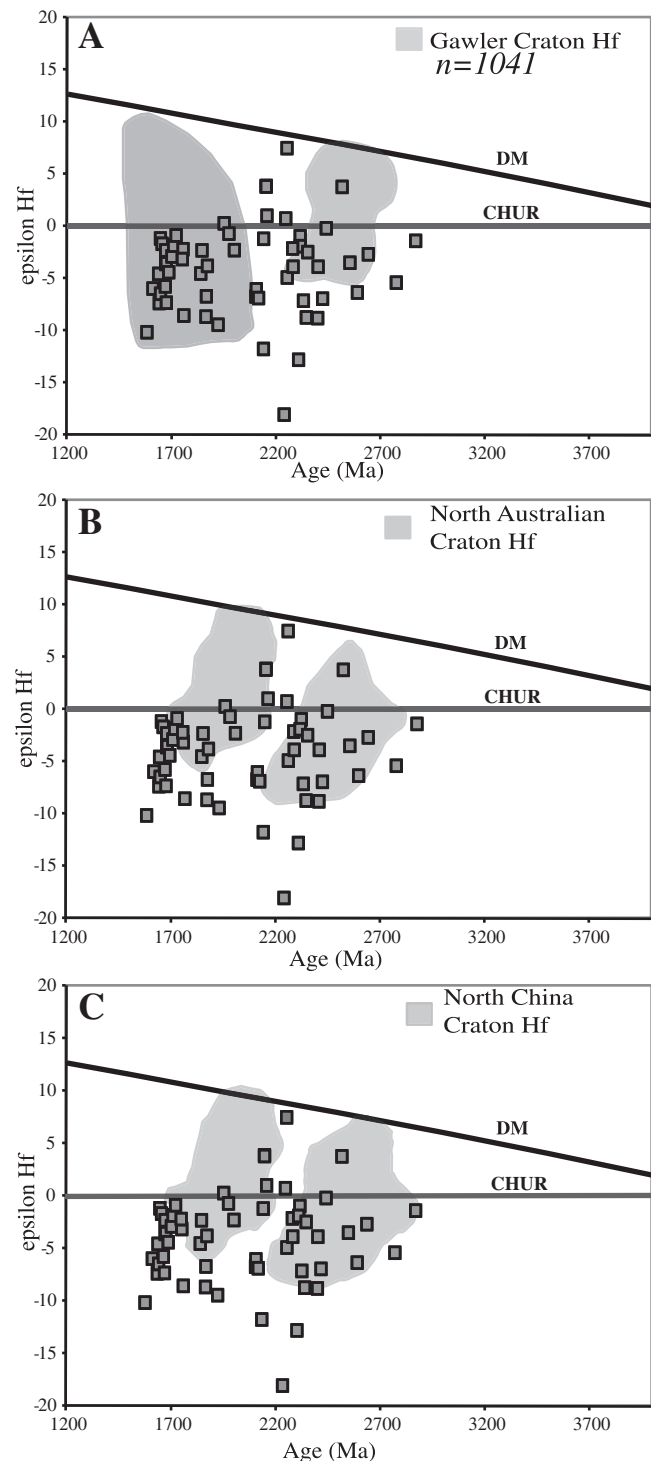


**Fig. 10.**  $\epsilon_{\text{Hf}}$  values plotted against  $^{207}\text{Pb}/^{206}\text{Pb}$  ages for individual zircon grains from three metasedimentary samples from the Ongole Domain (BH08, BH16, I0508). The shaded areas represent the hafnium isotope values reported for zircon grains from the Gawler Craton (A), the North Australian Craton (B) and the North China Craton (C). The hafnium values are compiled from Zhang et al. (2007), Belousova et al. (2009), Hollis et al. (2010), Howard et al. (2011), Wan et al. (2011), Yin et al. (2011), and Guitreau et al. (2012). N = number of analyses used to generate the hafnium fields.

the link plausible. However, it is worth considering that Proterozoic Australia also shows a number of geochronological and isotopic overlaps to the detrital populations observed in the Ongole Domain. It is possible that these regions may have been proximal to the Ongole Domain/Napier Complex in the late Palaeoproterozoic.

## 5.2. Magmatism in the Ongole Domain

The combined U–Pb and Lu–Hf zircon data from five igneous rocks in the Ongole Domain (Figs. 3 and 8) indicate that magmatism involved reworking of Archaean crust, with minor juvenile input. Previous U–Pb zircon and monazite studies have identified the emplacement of enderbites (charnockites) at 1720–1700 Ma (Kovach et al., 2001), anorthosite emplacement between 1690 and 1630 Ma (Dharma Rao et al., 2012) and granite emplacement between 1650 and 1450 Ma (Simmat and Raith, 2008). Overlapping magmatic ages between ca. 1640 and 1570 Ma in this study, as well as the previously published U–Pb zircon and monazite data, suggest that the Ongole Domain was magmatically active between at least ca. 1720 and 1570 Ma. In terms of inheritance, the igneous rocks preserve inherited grains that range between ca. 1880–1640 Ma. The late Palaeoproterozoic inherited grains record similar populations to those identified in the metasedimentary rocks in the Ongole Domain. However, the absence of any inherited Archaean grains in the magmatic rocks is a noticeable difference to the detrital zircon populations preserved in the Ongole Domain metasedimentary rocks.

Lu–Hf zircon isotope data from the Ongole Domain igneous zircon grains show that the parental magma was evolved, and became marginally more juvenile in the younger magmatic rocks (Fig. 8). Metamorphic zircon grains from the Ongole Domain metasedimentary rocks (ca. 1670–1590 Ma) yield  $\epsilon_{\text{HF}(T)}$  values between –7 and –1 (average = –5), whereas igneous zircon grains of the same age yield predominantly more evolved  $\epsilon_{\text{HF}(T)}$  values between –12 and –3 (average = –8). This implies that the igneous rocks could be sampling Archaean crust in the lower crustal column that may not necessarily be the metasedimentary rocks identified in this study. The lack of Archaean zircon inheritance in the felsic magmatic rocks also suggests that the metasedimentary rocks are unlikely to have contributed to the source of the magmatic rocks. Hf depleted mantle model ages in the analysed igneous zircon grains suggests the source of the magmatism incorporates reworking of Archaean crust with a minimum age of 2.7–2.5 Ga. Juvenile crust of this age is recognised in abundance in the neighbouring eastern Dharwar Craton (Jayananda et al., 2000). However, appropriately-aged Archaean crust is also exposed throughout the Napier Complex of East Antarctica (Boger, 2011; Horie et al., 2012; Mohanty, 2011). The igneous zircon data is therefore consistent with the interpreted Antarctic source for metasedimentary rock provenance.

## 5.3. Metamorphism in the Ongole Domain

Ultra high temperature (UHT) metamorphic conditions have been described in the several areas of the Ongole Domain (Dasgupta et al., 1997; Leelanandam, 1997; Sengupta et al., 1999; Bhui et al., 2007). Rocks from the contact zone around the Kondapalle Layered Complex preserve evidence for UHT conditions of >1000 °C and 10 kb (Sengupta et al., 1999), and the rocks at Chimakurthy record mid-crustal level conditions of >950 °C and 6 kb (Dasgupta et al., 1997). In both cases, the UHT conditions have been ascribed to heat supplied by mafic ultra-mafic magmatism, and are not considered to represent the conditions associated with regional granulite-facies metamorphism in the Ongole Domain. The timing of metamorphism has been reported to be generally between ca. 1700–1512 Ma (Kovach et al., 2001; Mukhopadhyay and Basak, 2009; Upadhyay et al., 2009). The broad range of ages is likely attributed to isotopic disturbance of monazite and zircon grains during prolonged periods of granulite-facies metamorphism (Booth et al., 2005). Upadhyay et al. (2009) reported total resetting of the U–Pb systems, and disturbance of REEs and Hf isotopes, from detrital zircons in the Ongole Domain during metamorphism at ca. 1630 Ma. Combined zircon and monazite studies are widely used to place temporal constraints on metamorphism; however, at granulite-facies conditions they are vulnerable to diffusion (Rubatto et al., 2001). As such, deciphering a geologically sound meaning from the zircon and monazite data obtained in this study is approached with caution. The combined metamorphic monazite and

zircon data form a largely bimodal population (zircon growth dominates the period between ca. 1680–1630 Ma, and monazite at ca. 1590 Ma) and can be interpreted in one of two ways: 1) a protracted metamorphic event, or a number discrete events occurred between 1680 Ma and 1590 Ma; or 2) the dominant metamorphic event occurred at ca. 1590 Ma and the broad smear of zircon data between ca. 1680 and 1590 Ma reflects disturbance and resetting of the isotopic clocks.

A systematic process was used to interpret the U–Pb zircon data; integrating the internal textures acquired from CL images and the Th/U contents of the zircon grains. The CL images reveal that zircon grains extracted from the igneous and metasedimentary rocks consistently preserve evidence for complex isotopic disturbance (Fig. 5). Magmatic zircon grains typically exhibit well developed oscillatory zoning (Corfu et al., 2003). Ongole Domain zircon grains from both igneous and metasedimentary rocks invariably preserve some growth zoning, but particularly in the metasedimentary zircon grains, zoning is largely disturbed, blurred, or truncated by homogenous weakly to strongly luminescent fronts; features commonly attributed to overprinting during high grade metamorphism (Hoskin and Black, 2000; Hoskin and Schaltegger, 2003; Hofmann et al., 2009; Flowers et al., 2010), or disturbance within the zircon crystal during the final stages of magmatic cooling (Harley and Black, 1997; Pidgeon et al., 1998; Corfu et al., 2003).

The ratio of Th to U in zircon is used as a guide for differentiating between magmatic and metamorphic zircon (Harley and Black, 1997; Pidgeon et al., 1998; Rubatto et al., 2001; Rubatto, 2002; Corfu et al., 2003). Zircon grains within the Ongole Domain igneous rocks have Th/U ratios (Fig. 11A) consistent with those crystallised during magmatic processes (e.g. Th/U ratio > 0.5, Xiang et al., 2011). Zircon grains from the Ongole Domain metasedimentary rocks aged between ca. 1700–1600 Ma yield a broad spectrum of Th/U ratios between 0.01 and 0.7 (Fig. 11B). Analyses from metamorphic rims and homogenous grains consistently exhibit ratios below <0.2, suggesting that the growth of zircon is concurrent with metamorphism (Schaltegger et al., 1999; Hoskin and Black, 2000; Rubatto, 2002).

Within all three metasedimentary rocks in the Ongole Domain, oscillatory-zoned cores record a unimodal population of  $1720 \pm 18$  Ma, which is interpreted to represent the maximum age of deposition of the protolith sedimentary rocks. All metasedimentary grains younger than this preserve evidence for isotopic disturbance; in both distinct CL characteristics (Fig. 5) and low Th/U ratios (Fig. 11B). An attempt to further refine the timing of metamorphism in the Ongole Domain is hindered by a broad smear of concordant zircon data between 1680 and 1580 Ma (Fig. 4).

A number of scenarios could have contributed to the continual crystallisation of metamorphic zircon over the period between ca. 1680–1580 Ma. Solid-state recrystallisation (Corfu et al., 2003; Hoskin and Schaltegger, 2003), coupled-dissolution reprecipitation (Geisler et al., 2007), zircon growth at the onset of anatexis (Roberts and Finger, 1997), or zircon growth resulting from the breakdown of zirconium-bearing minerals such as ilmenite and garnet (Fraser et al., 1997; Degeling et al., 2001; Geisler et al., 2007) are possible processes that would yield variable isotopic records during a granulite-facies event. Closed system, solid-state recrystallisation has been shown to produce blurred primary zones, patchy zoning, and “ghost” zoning in granulite-facies zircon crystals (Tichomirowa et al., 2005); internal features seen frequently within the Ongole Domain zircon grains (Table 2, Fig. 5). On the basis of CL image analysis, the preferred interpretation for the mechanism driving isotopic disturbance in the zircon grains is solid-state recrystallisation; resulting in the cross cutting ghost zones and homogenous rims preserved on a high percentage of the metasedimentary zircon grains. Heterogeneous lead loss has been previously documented in solid-state recrystallised granulite-facies zircon grains (Flowers et al., 2010; Kryza et al., 2012; Wan et al., 2011).

In order to best interpret the data, interpreted metamorphic zircon analyses were filtered to exclude U–Pb ages >2% discordant. Upon

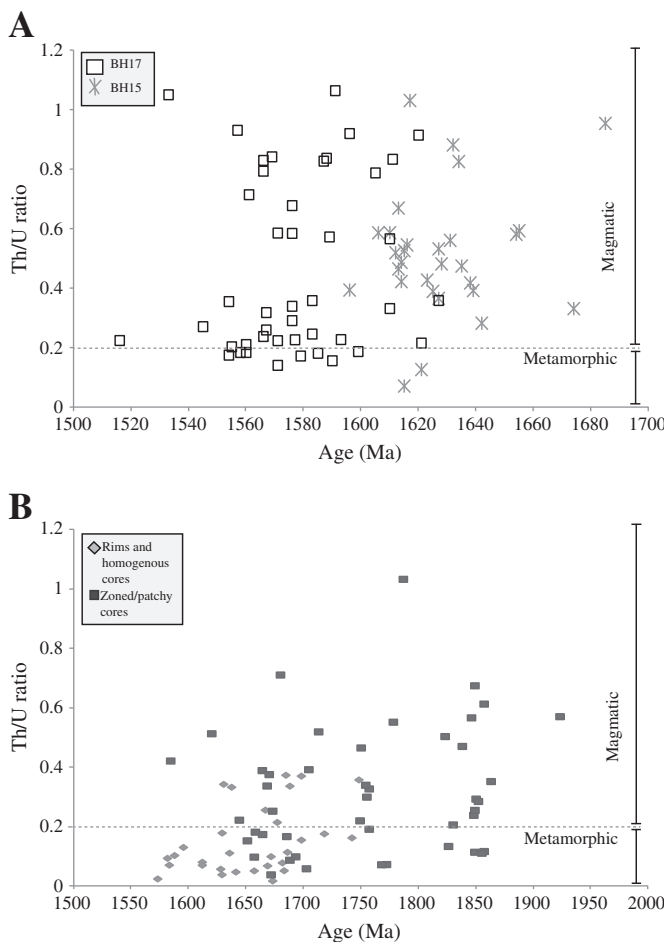


**Fig. 11.** Th/U ratio versus  $^{207}\text{Pb}/^{206}\text{Pb}$  age for selected zircon analyses from A) igneous samples BH15 and BH17. All analyses are from oscillatory zoned zircon grains. B) Metasedimentary samples BH08, BH16 and I0508. Data is displayed in accordance with the CL domain targeted during analysis; these are oscillatory zoned and blurry zoned cores, or metamorphic rims and homogenous grains. The line represents the distinction between 'metamorphic' and 'igneous' zircon grains.

filtering, concordant metamorphic zircon forms a continuous spread between ca. 1700 and 1590 Ma, with a small population between ca. 1580–1570 Ma (Fig. 12A). Of these data, rim analyses form two distinct populations at  $1633 \pm 12$  Ma and  $1670 \pm 14$  Ma, with two younger outliers at  $1573 \pm 19$  and  $1600 \pm 18$  Ma (Fig. 12B). Homogenous and blurred cores yield a broad spread of ages between ca. 1700 and 1580 Ma, with major populations at  $1689 \pm 8$  Ma and  $1639 \pm 9$  Ma (Fig. 12C). The data are asymmetrically skewed towards the late Palaeoproterozoic ages with a small population of outliers yielding a unimodal population of  $1590 \pm 16$  Ma, overlapping with the dominant monazite ages found in the same rocks. The trace element composition of the zircon grains from garnet bearing, metasedimentary samples BH16 and BH08 was also analysed (supplementary data). The REE composition of zircon grains can be used to link the paragenesis of the zircons to the timing and conditions of metamorphism (Rubatto et al., 2001; Rubatto, 2002; Hanchar and van Westrenen, 2007). From the concordant ( $\pm 2\%$ ) ca. 1670 Ma zircon rim population, a small number of analyses from the garnet-bearing sample BH16 exhibit HREE depletion (supplementary data). This pattern indicates possible concurrent metamorphic zircon and garnet porphyroblast growth during this period (individual zircon ages are 1669, 1667 and 1650 Ma). In a closed system, coexisting zircon and garnet will compete for HREE as the trace element reservoir is limited; consequently, metamorphic zircon will yield HREE depleted patterns (Rubatto, 2002). HREE depleted metamorphic zircon growth at ca. 1660 Ma could indicate that the zircon grew concurrently with

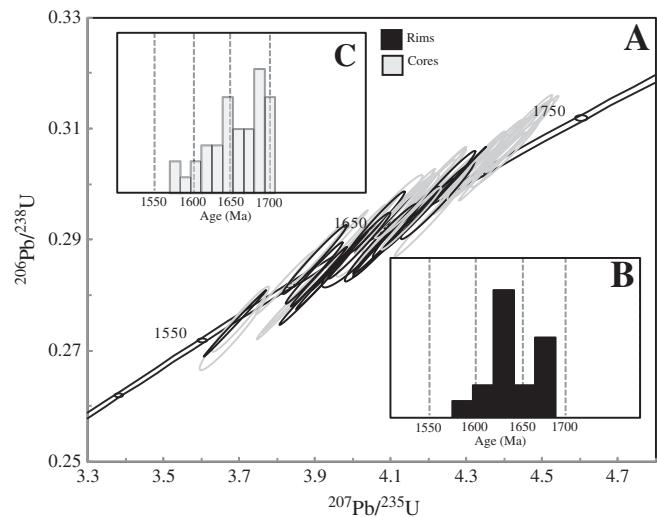


**Fig. 12.** A) Concordia diagram showing metasedimentary zircon grains of  $<2\%$  discordancy, from Ongole Domain samples BH08, BH16 and I0508. Rim analyses are indicated in black, core analyses are indicated in grey. B) Histogram of ages of rim analyses from  $<2\%$  discordant grains in samples BH08, BH16, I0508. C) Probability density plot of core analyses from  $<2\%$  discordant grains in samples BH08, BH16, I0508.

another mineral that exhibits a high partition coefficient of HREE, such as garnet (Rubatto, 2002).

Continual or intermittent zircon growth during prolonged metamorphic events has been previously documented in high grade terranes (Ashwal et al., 1999; Bomparola et al., 2007; Claué-Long et al., 2008b; Högdahl et al., 2011). The presence of additional sources of heat and/or heat transport, such as the emplacement of magmatic bodies, can also contribute thermal pulses to mountain building cycles and result in heterogeneous crystallisation ages in zircon (Santosh et al., 2006; Zeh et al., 2003). Magmatic intrusions were emplaced in the Ongole Domain over a minimum period of 70 million years (ca. 1640–1570 Ma, present study), in addition to ultra-mafic-mafic intrusions (Sengupta et al., 1999; Dharma Rao et al., 2012). The magmatic activity potentially provide an intermittent source of advective heat and fluids, which may have encouraged intermittent zircon growth over a minimum ~70 Myr period (see Ashwal et al., 1999).

The monazite data present a slightly different story to that of the zircon data (Fig. 6). The majority of monazites in the metasedimentary rocks indicate a major growth event at ca. 1590 Ma. A small population of older concordant monazite grains in sample BH16 (ca. 1680–1640 Ma) are hosted in garnet grains. The age ranges of the older grains overlap with the ages of metamorphic zircon recognised in the same rocks. The preservation of older monazite grains within garnet porphyroblasts has been previously documented (Montel et al., 2000; Forbes et al., 2007), and could be attributed to the textural location of the monazites. The oldest population are armoured within garnets grains, which could have provided protection against tectonothermal disturbance (Forbes et al., 2007).

The discrepancy between the dominant monazite and zircon ages is not unusual in the rock record, and a number of studies have reported this occurrence (Kiny et al., 1999; Aleinikoff et al., 2000; Zeh et al., 2003). In most cases the difference between older zircon growth ages and younger monazite ages are attributed to partial to complete isotopic resetting, discordancy or polymetamorphic events. Kelsey et al. (2008) suggests the gap in ages recorded by monazite and zircon reflect growth behaviour of the minerals rather than differences in closure temperatures. If the temperature rate at which zircon and monazite growth occurred was significantly different, the geochronometers will preserve difference points in the evolution of the orogen. At temperatures above ~700–780 °C in monazite saturated rocks, where melt loss does not occur; monazite will dissolve completely and will recrystallise upon cooling below the solidus. Therefore, the dominant ca. 1590 Ma monazite

population could represent the rocks passing through the closure temperature of ~780–700 °C (Kelsey et al., 2008). Hence, the oldest monazite inclusions (shielded within garnets) could record growth along the prograde path of a long, hot orogen (Melleton et al., 2009), and the younger grains along the retrograde path.

The timing of granulite facies metamorphism in the Ongole Domain is variably reported to have occurred at 1.76 Ga (Bose et al., 2011), 1.63–1.61 Ga (Upadhyay et al., 2009) and 1.65–1.59 Ga (Simmat and Raith, 2008). The combined U–Pb zircon and monazite geochronology, Th/U and REE trace element data from this study suggest that metamorphism commenced by ca. 1.68–1.67 Ga, coinciding with oldest monazite grains in garnet and the HREE depleted zircon rims, and continued until 1.59 Ga. It is also plausible that a percentage of the metamorphic ages between ca. 1.68–1.60 Ma are the result of partial resetting, or mixed ages (Hoskin and Black, 2000), leading down to a major event at 1.59 Ga.

#### 5.4. Regional and palaeogeographic implications

This study presents the first comprehensive combined U–Pb geochronology and Hf isotope provenance study for the metapelitic rocks

in the Ongole Domain, which, coupled with data on igneous rocks, allows us to refine evolutionary models for the Ongole Domain.

At present two contrasting evolutionary models are considered for the Southern Eastern Ghats Belt (encompassing the Ongole Domain). The first proposed by Dharma Rao et al. (Fig. 15; 2011a) envisions a Mesoproterozoic active continental margin along the southeastern margin of India, generating subduction-related continental arc magmatism (Dharma Rao et al., 2013) and the accretion of a juvenile island arc; prior to terminal continent–continent collision in the Neoproterozoic amalgamation of the supercontinent Rodinia. Vijaya Kumar et al. (2011) propose that active margin tectonics along in the Mesoproterozoic led to the accretion of an island arc, followed by the generation of a continental magmatic arc (Kondapalle Magmatic arc), prior to terminal continent–continent collision at ca. 1.6 Ga. The authors attributed younger Mesoproterozoic events (1.5–1.3 Ga) to rifting parallel to the accreted margins. Dasgupta et al. (2013) endorse this model and suggest that although younger ages have been recognised throughout the Ongole Domain, the region was largely cratonised by ca. 1.6 Ga. We use the data collected in this study, in conjunction with existing data in the literature, to build

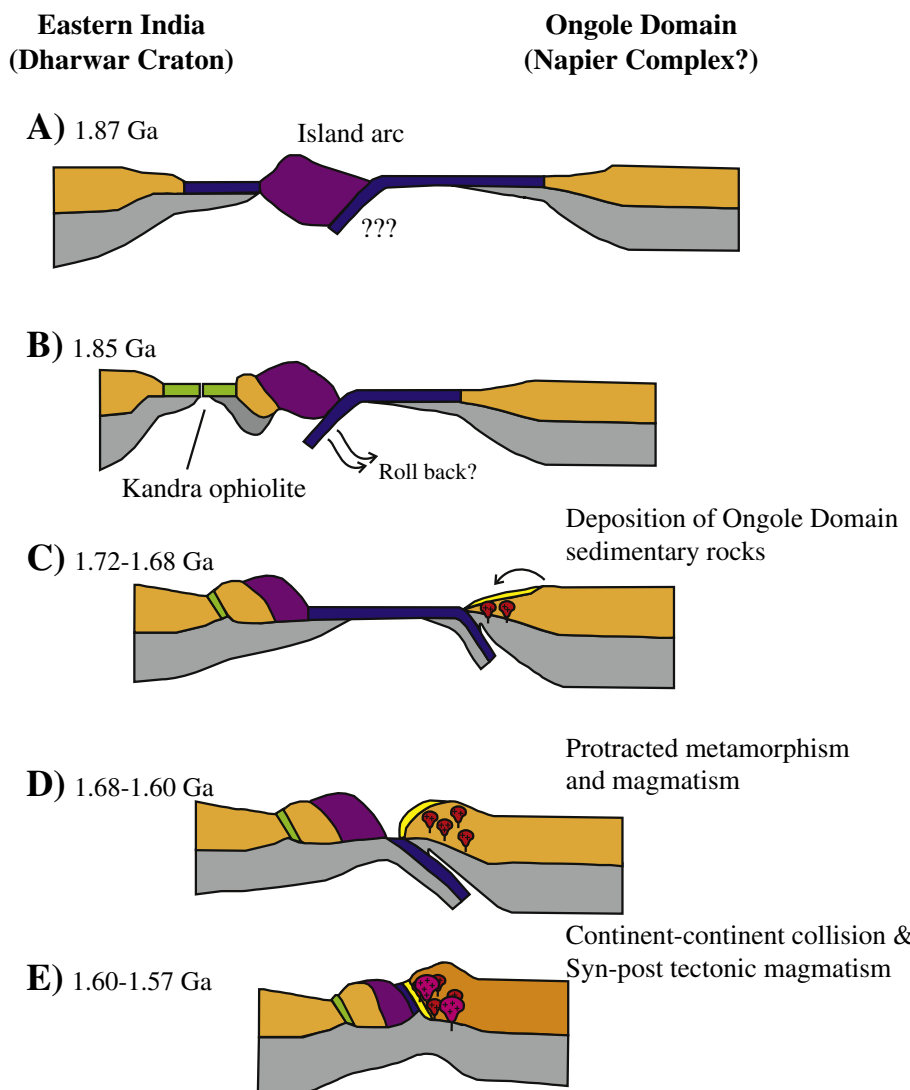


**Fig. 13.** Tectonic cartoon for the Palaeoproterozoic evolution of the Ongole Domain in eastern India (modified after Vijaya Kumar et al., 2011). (A) Following continental rifting at 1.89 Ga, oceanic crust is generated along the south-eastern margin of India (French et al., 2008). Oceanic decoupling (not shown) initiated subduction in the newly formed oceanic crust, resulting in the formation of an oceanic island arc. (B) Proposed subduction roll back in the Indian plate induces extension and subsequent development of the Kandra back arc basin ophiolite complex (Kumar et al., 2010). (C) Deposition of the Ongole Domain sedimentary protolith rocks occurs after 1.72 Ga. The most likely source is the Napier Complex. (D) Metamorphism and magmatism associated with accretionary orogenesis occurs between 1.68 and 1.60 Ga (present study, Dobmeier and Raith, 2003; Simmat and Raith, 2008; Mukhopadhyay and Basak, 2009; Dasgupta et al., 2013). (E) Collision of an exotic terrane hosting the Ongole Domain occurs by 1.6 Ga. Syn-post tectonic magmatism continues until 1.57 Ga.

on the model proposed by Vijaya Kumar et al. (2011) and Dasgupta et al. (2013).

Within the recognised proto-India portion of the Eastern Ghats Belt (i.e. Dharwar Craton plate) a major episode of passive rifting and intracontinental mafic magmatism along the SE margin of the Indian proto-continent has been interpreted at ca. 1890–1870 Ga (Chatterjee and Bhattacharji, 2001; French et al., 2008). Oceanic decoupling initiated subduction in the newly formed oceanic crust, and is interpreted to have resulted in the formation of an oceanic island arc (Fig. 13A; Dharm Rao et al., 2011a; Vijaya Kumar et al., 2011). Westward migration of subduction resulted in the accretion of the oceanic island arc to the rifted margin of proto-India (Fig. 13B; Dharm Rao et al., 2011a; Vijaya Kumar et al., 2011). On the basis of geochemical and geochronological analysis, further rifting along the SE margin of India led to the production of oceanic crust (Kandra Ophiolite Complex, Fig. 12B, Kumar et al., 2010), in a suprasubduction-zone setting, typical of a continental back arc basin (Kumar et al., 2010; Dharm Rao et al., 2011a; Saha, 2011). However, the driving mechanisms (i.e. slab pull vs. slab roll back and subduction polarity) behind the formation of the back arc basin is highly speculative (Dharm Rao et al., 2011a; Saha, 2011). Closure of the proposed back-arc basin is interpreted to have occurred either immediately after its formation (picture option in Fig. 13C, Vijaya Kumar et al., 2011) or during subsequent accretion of the Ongole Domain crust at ca. 1.6 Ga.

The first recorded event within the Ongole Domain is the deposition of the protolith sedimentary rocks occurred between ca. 1720 and 1670 Ma (Fig. 13C). Previous investigators have suggested that the sediments were likely to have been derived from the Dharwar Craton (Rickers et al., 2001), but the detrital zircon data presented in this study contradict this, with rocks of the Napier Complex suggested as sources of detritus. We suggest that the lack of Dharwar Craton detritus, coupled with the recorded suture between the Ongole Domain and NSB, indicates that the Ongole Domain was exotic to the Dharwar Craton/proto-India at the time of sediment deposition (ca. 1720 Ma, Fig. 13C).

Previous studies suggest magmatism commenced in the Ongole Domain as early as 1720 Ma (Rickers et al., 2001), and persisted continuously, or episodically, until at least 1570 Ma (Fig. 13C–E). The results of this study suggest that metamorphism commenced by ca. 1.67 Ga and is recorded by monazite grains in garnet, and the coeval growth of metamorphic zircon rims. The tectonothermal activity is interpreted to culminate in terminal collisional orogenesis at ca. 1.6–1.59 Ga (Fig. 13E; Vijaya Kumar et al., 2010). As pictured in Fig. 13, most authors attribute the prolonged magmatic and metamorphic activity during this interval to be the result of on-going subduction related activity (Dobmeier and Raith, 2003; Bose et al., 2011; Vijaya Kumar et al., 2011; Dharm Rao et al., 2012; Dasgupta et al., 2013; Dharm Rao et al., 2013). However, the lack of identifiable magmatism in the NSB at this time is perhaps also consistent with subduction under the Ongole Domain prior to collision (Fig. 13C–E). Alkaline magmatism is subsequently recorded in the Ongole Domain between ca. 1600 and 1350 Ma, which is interpreted to have been emplaced in a post-orogenic setting (Fig. 13E, Dobmeier et al., 2006; Vijaya Kumar et al., 2011). In the proposed model, the Ongole Domain forms the leading edge of the Napier Complex crustal block (Dobmeier and Raith, 2003; Upadhyay et al., 2009). Evidence for ca. 1.6 Ga metamorphic and magmatic activity have been found in the Oygarden Group in the Napier Complex (Kelly et al., 2002), adding support to the Mesoproterozoic link between India and the Napier Complex.

Palaeogeographic and palaeomagnetic data suggest that proto-India formed an integral part of the supercontinent Columbia, which amalgamated between ca. 1.9 and 1.8 Ga and rifted apart between 1.5 and 1.25 Ga (Rogers and Santosh, 2002; Zhao et al., 2004; Hou et al., 2008; Evans and Mitchell, 2011). Zhang et al. (see Fig. 7, 2012) present high-quality palaeomagnetic data for the North China Block during the time interval ca. 1780–1440 Ma, and place western India adjacent to the North China Block. In this reconstruction of Columbia, India appears

adjacent to North Australia and the North China Craton on the interior of the supercontinent (Zhang et al., 2012). In this model Laurentia, Baltica, Siberia and North China are palaeomagnetically well constrained, whereas India is relatively poorly constrained by two poles at ca. 1800 Ma. Such an interpretation is at odds with interpreted ophiolite complexes at Kanigiri and Kandra (Vijaya Kumar et al., 2010; Dharm Rao et al., 2011a), extensive metamorphism and geochemical evidence for continental arc-magmatism in the Kondapalle mafic complex (Dharm Rao and Santosh, 2011), which all suggest a plate margin location for proto-India during the late Palaeo- to early Mesoproterozoic.

In contrast, Pisarevsky et al. (2013) present palaeomagnetic and geochronological data from the Mesoproterozoic Lakhna dykes in the Bastar Craton (attached at the time to the Dharwar Craton) to support a ca. 1460 Ma palaeo-position whereby western India is juxtaposed against south-west Baltica. In this model, eastern India, south-eastern Laurentia and south-west Baltica represent a long lived, linear accretionary orogen. Pisarevsky et al. (2013) support the ca. 1.85–1.33 Ga on-going accretionary orogenesis suggested by Dharm Rao et al. (2011a). However, this scenario does not take into account the granulite-facies metamorphic event recorded between ca. 1.6 Ga which appears to be the dominant, and potentially the only tectonic event in the period 1.8–1.33 Ga that is consistent with accretionary or collisional processes. To resolve the conflicts between the Pisarevsky et al. (2013) and Vijaya Kumar et al. (2011) models we propose the scenario depicted in Fig. 14. In this reconstruction eastern India forms part of a linear accretionary system encompassing south-eastern Laurentia and Baltica. This model accounts for the magmatism and metamorphism recorded in the Ongole Domain between 1.72 and 1.6 Ga leading up to continent–continent collision. We suggest subduction stepped outboard

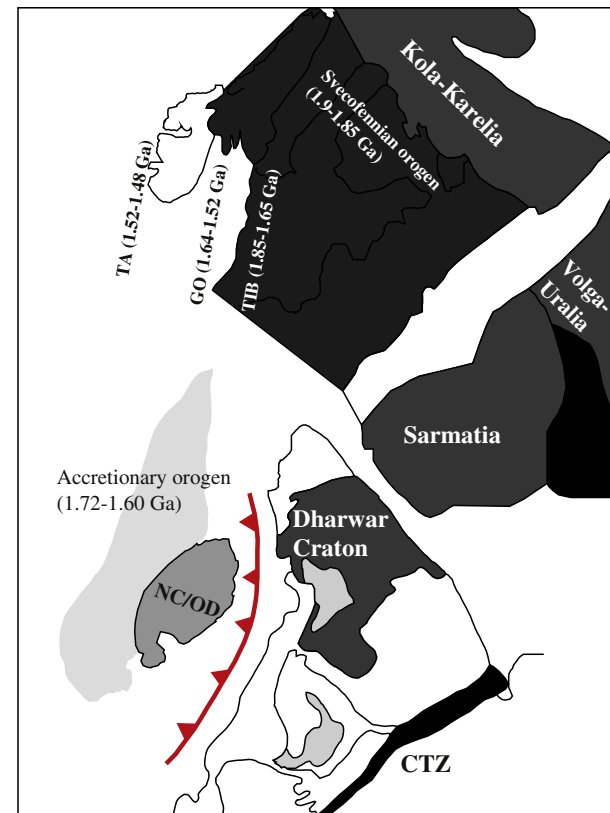


**Fig. 14.** Palaeogeographic reconstruction of the potential position of proto-India and the Ongole Domain within the supercontinent Nuna, modified after Pisarevsky et al. (2012). The following abbreviations have been used: SNO – Sveconorwegian orogeny; TA – Telemarkian accretionary events; GO – Gothian Orogeny; CTZ – Central Tectonic Zone; TIB – Transcandinavian Igneous Belt; NC – Napier Complex; OD – Ongole Domain; NAC – North Australian Craton.

(i.e. to the south with respect to present-day Indian coordinates) after a continent containing the Ongole Domain and Napier Complex collided with SE proto-India at ca. 1.6 Ga. Accretionary orogenesis could then feasibly be terminated by the collision that developed the northern Eastern Ghats-Rayner Orogen in east India/Antarctica at ca. 1 Ga ([Mezger and Cosca, 1999b](#); [Dobmeier and Raith, 2003](#)).

## 6. Conclusions

U-Pb detrital zircon data indicate deposition of the sedimentary protolith rocks in the Ongole Domain occurred between ca. 1.72 and 1.68 Ga. Detrital zircon patterns are dominated by Palaeoproterozoic grains and minor populations of Neoarchaean grains. The combined U-Pb and Lu-Hf isotope data from the detrital zircon grains suggest that the protolith sedimentary rocks were not derived from the Dharwar Craton, as had been previously assumed. Instead the most likely source region is from the Napier Complex (Antarctica). Similarities in U-Pb and Hf data between the Ongole Domain protoliths and metasedimentary protoliths from the North Australian Craton, suggest they may share this Antarctic source. Metamorphism between 1.68 and 1.6 Ga resulted in partial to complete resetting of zircon grains via solid state recrystallisation, as well as the growth of new metamorphic zircon during two distinct periods at ca. 1.67 and 1.63 Ga. Metamorphic zircon during these periods is characterised by the growth of featureless grains and rims on pre-existing zircon grains. In-situ monazite geochronology from metasediments preserves early phases of metamorphism at 1.68–1.64 in monazite grains armoured in garnets, and a major period of monazite crystallisation between 1.6 and 1.59 Ga.

Felsic magmatism in the Ongole Domain occurred episodically between 1.64 and 1.57 Ga, yielding felsic opx-bearing granitoids. Isotopically, the granitoids are evolved yielding  $\epsilon\text{Hf}$  values in zircon between –2 and –12. The magmatism is interpreted to have been derived from the reworking of Archaean crust with only minor juvenile input. In light of the data obtained, as well as recent palaeomagnetic constraints, we propose a new model for the evolution of the Ongole Domain. The model suggests the Ongole Domain represents a fraction of an exotic terrane that was transferred to proto-India in the late Palaeoproterozoic (1.68–1.6 Ga), as part of a linear accretionary orogenic belt that also encompassed south-west Baltica and south-eastern Laurentia. The combined U-Pb–Hf detrital and igneous zircon data support the existing hypothesis that the exotic terrane accreted to the Eastern Ghats Belt at ca. 1.6 Ga is the Napier Complex, Antarctica but also suggests that this may have been connected to parts of Proterozoic Australia.

## Acknowledgements

This project was financed by the Australian and Indian Governments through Australia–India Strategic Research Fund grant #ST030046 and the Australian Research Council grant FT120100340. BH is also funded by an Australian Postgraduate Award. We would like to thank Dr. Sarbani Patranabis-Deb (IIT Kharagpur) for her hospitality and help during fieldwork and Ryan Gore, Georgy Falster, Emma Alexander and Andrew Barker for assistance in the field. Ben Wade and Angus Netting provided vital support for U-Pb geochronology. We would like to thank Professor Santosh for efficient editing and Chris Clark and an anonymous reviewer whose comments improved this manuscript. This paper forms TRaX Record #273.

## Appendix A. Supplementary data

Supplementary data to this article can be found online at <http://dx.doi.org/10.1016/j.gr.2013.09.002>.

## References

- Aleinikoff, J.N., Burton, W.C., Lytle, P.T., Nelson, A.E., Southworth, C.S., 2000. U-Pb geochronology of zircon and monazite from Mesoproterozoic granitic gneisses of the northern Blue Ridge, Virginia and Maryland, USA. *Precambrian Research* 99, 113–146.
- Asami, M., Suzuki, K., Grew, E.S., 2002. Chemical Th-U-total Pb dating by electron microprobe analysis of monazite, xenotime and zircon from the Archean Napier Complex, East Antarctica: evidence for ultra-high-temperature metamorphism at 2400 Ma. *Precambrian Research* 114, 249–275.
- Ashwal, L.D., Tucker, R.D., Zinner, E.K., 1999. Slow cooling of deep crustal granulites and Pb-loss in zircon. *Geochimica et Cosmochimica Acta* 63, 2839–2851.
- Belousova, E.A., Reid, A.J., Griffin, W.L., O'Reilly, S.Y., 2009. Rejuvenation vs. recycling of Archean crust in the Gawler Craton, South Australia: evidence from U-Pb and Hf isotopes in detrital zircon. *Lithos* 113, 570–582.
- Betts, P.G., Giles, D., 2006. The 1800–1100 Ma tectonic evolution of Australia. *Precambrian Research* 144, 92–125.
- Bhowmik, S.K., Dasgupta, S., 2012. Tectonothermal evolution of the Banded Gneissic Complex in central Rajasthan, NW India: present status and correlation. *Journal of Asian Earth Sciences* 49, 339–348.
- Bhui, U.K., Sengupta, P., Sengupta, P., 2007. Phase relations in mafic dykes and their host rocks from Kondapalle, Andhra Pradesh, India: implications for the time-depth trajectory of the Palaeoproterozoic (late Archaean?) granulites from southern Eastern Ghats Belt. *Precambrian Research* 156, 153–174.
- Boger, S.D., 2011. Antarctica – Before and after Gondwana. *Gondwana Research* 19, 335–371.
- Bomparola, R.M., Ghezzo, C., Belousova, E., Griffin, W.L., O'Reilly, S.Y., 2007. Resetting of the U-Pb Zircon System in Cambro-Ordovician Intrusives of the Deep Freeze Range, Northern Victoria Land, Antarctica. *Journal of Petrology* 48, 327–364.
- Booth, A.L., Kolodny, Y., Chamberlain, C.P., McWilliams, M., Schmitt, A.K., Wooden, J., 2005. Oxygen isotopic composition and U-Pb discordance in zircon. *Geochimica et Cosmochimica Acta* 69, 4895–4905.
- Bose, S., Dunkley, D.J., Dasgupta, S., Das, K., Arima, M., 2011. India–Antarctica–Australia-Laurentia connection in the Palaeoproterozoic–Mesoproterozoic revisited: evidence from new zircon U-Pb and monazite chemical age data from the Eastern Ghats Belt, India. *Geological Society of America Bulletin* 123, 2031–2049.
- Carson, C.J., Ague, J.J., Coath, C.D., 2002. U-Pb geochronology from Tonagh Island, East Antarctica: implications for the timing of ultra-high temperature metamorphism of the Napier Complex. *Precambrian Research* 116, 237–263.
- Cawood, P.A., Korsch, R.J., 2008. Assembling Australia: Proterozoic building of a continent. *Precambrian Research* 166, 1–35.
- Chatterjee, N., Bhattacharji, S., 2001. Petrology, geochemistry and tectonic settings of the mafic dikes and sills associated with the evolution of the Proterozoic Cuddapah Basin of South India. *Proceedings of the Indian Academy of Sciences, Earth and Planetary Sciences* 110, 433–453.
- Claoué-Long, J., Edgose, C., Worden, K., 2008a. A correlation of Aileron Province stratigraphy in central Australia. *Precambrian Research* 166, 230–245.
- Claoué-Long, J., Maidment, D., Hussey, K., Huston, D., 2008b. The duration of the Strangways Event in central Australia: evidence for prolonged deep crust processes. *Precambrian Research* 166, 246–262.
- Collins, A.S., Pisarevsky, S.A., 2005. Amalgamating eastern Gondwana: the evolution of the Circum-Indian Orogens. *Earth-Science Reviews* 71, 229–270.
- Corfu, F., Hanchar, J.M., Hoskin, P.W.O., Kinny, P.D., 2003. Atlas of zircon textures. *Zircon* 53, 468–500.
- Cross, A.J., Crispe, A.J., 2007. SHRIMP U-Pb analyses of detrital zircon: a window to understanding the Palaeoproterozoic development of the Tanami Region, northern Australia. *Mineralium Deposita* 42, 27–50.
- Dasgupta, S., Ehl, J., Raith, M.M., Sengupta, P., Sengupta, P., 1997. Mid-crustal contact metamorphism around the Chikmagalur mafic-ultramafic complex, Eastern Ghats Belt, India. *Contributions to Mineralogy and Petrology* 129, 182–197.
- Dasgupta, S., Bose, S., Das, K., 2013. Tectonic evolution of the Eastern Ghats Belt, India. *Precambrian Research* 227, 247–258.
- Degeling, H., Eggins, S., Ellis, D.J., 2001. Zr budgets for metamorphic reactions, and the formation of zircon from garnet breakdown. *Mineralogical Magazine* 65, 749–758.
- Dharma Rao, C.V., Reddy, U.V.B., 2009. Petrological and geochemical characterization of Proterozoic ophiolitic mélange, Nellore–Khammam schist belt, SE India. *Journal of Asian Earth Sciences* 36, 261–276.
- Dharma Rao, C.V., Santosh, M., 2011. Continental arc magmatism in a Mesoproterozoic convergent margin: petrological and geochemical constraints from the magmatic suite of Kondapalle along the eastern margin of the Indian plate. *Tectonophysics* 510, 151–171.
- Dharma Rao, C.V., Santosh, M., Wu, Y.-B., 2011a. Mesoproterozoic ophiolitic mélange from the SE periphery of the Indian plate: U-Pb zircon ages and tectonic implications. *Gondwana Research* 19, 384–401.
- Dharma Rao, C.V., Windley, B.F., Choudhary, A.K., 2011b. The Chimalpahad anorthosite Complex and associated basaltic amphibolites, Nellore Schist Belt, India: magma chamber and roof of a Proterozoic island arc. *Journal of Asian Earth Sciences* 40, 1027–1043.
- Dharma Rao, C.V., Santosh, M., Dong, Y., 2012. U-Pb zircon chronology of the Pangidi–Kondapalle layered intrusion, Eastern Ghats belt, India: constraints on Mesoproterozoic arc magmatism in a convergent margin setting. *Journal of Asian Earth Sciences* 49, 362–375.
- Dharma Rao, C.V., Santosh, M., Zhang, Z., Tsunogae, T., 2013. Mesoproterozoic arc magmatism in SE India: Petrology, zircon U-Pb geochronology and Hf isotopes of the Bopudi felsic suite from Eastern Ghats Belt. *Journal of Asian Earth Sciences* 75, 183–201.
- Dobmeier, C., Raith, M., 2003. Crustal architecture and evolution of the Eastern Ghats Belt and adjacent regions of India. In: Yoshida, M., Windley, B.F., Dasgupta, S. (Eds.), *Proterozoic East Gondwana: supercontinent assembly and breakup*. Geol.Soc., London Sp. Publ, pp. 145–168.

- Dobmeier, C., Lutke, S., Hammerschmidt, K., Mezger, K., 2006. Emplacement and deformation of the Vinukonda meta-granite (Eastern Ghats, India) – implications for the geological evolution of peninsular India and for Rodinia reconstructions. *Precambrian Research* 146, 165–178.
- Ernst, R.E., Wingate, M.T.D., Buchan, K.L., Li, Z.X., 2008. Global record of 1600–700 Ma Large Igneous Provinces (LIPs): implications for the reconstruction of the proposed Nuna (Columbia) and Rodinia supercontinents. *Precambrian Research* 160, 159–178.
- Evens, D.A.D., Mitchell, R.N., 2011. Assembly and breakup of the core of Palaeoproterozoic–Mesoproterozoic supercontinent Nuna. *Geology* 39, 443–446.
- Flowers, R.M., Schmitt, A.K., Grove, M., 2010. Decoupling of U–Pb dates from chemical and crystallographic domains in granulite facies zircon. *Chemical Geology* 270, 20–30.
- Forbes, C.J., Giles, D., Betts, P.G., Weinberg, R., Kinny, P.D., 2007. Dating prograde amphibolite and granulite facies metamorphism using *in situ* monazite U–Pb SHRIMP analysis. *Journal of Geology* 115, 691–705.
- Fraser, G., Ellis, D., Eggins, S., 1997. Zirconium abundance in granulite-facies minerals, with implications for zircon geochronology in high-grade rocks. *Geology* 25, 607–610.
- French, J.E., Heaman, L.M., 2010. Precise U–Pb dating of Paleoproterozoic mafic dyke swarms of the Dharwar craton, India: implications for the existence of the Neoarchean supercraton Slavia. *Precambrian Research* 183, 416–441.
- French, J.E., Heaman, L.M., Chacko, T., Srivastava, R.K., 2008. 1891–1883 Ma Southern Bastar–Cuddapah mafic igneous events, India: a newly recognized large igneous province. *Precambrian Research* 160, 308–322.
- Geisler, T., Schaltegger, U., Tomaschek, F., 2007. Re-equilibration of zircon in aqueous fluids and melts. *Elements* 3, 43–50.
- Grew, E.S., Suzuki, K., Asami, M., 2001. CHIME ages of xenotime, monazite and zircon from beryllium pegmatites in the Napier Complex, Khmara Bay, Enderby Land, East Antarctica. *Polar Geoscience* 14, 99–118.
- Griffin, W.L., Wang, X., Jackson, S.E., Pearson, N.J., O'Reilly, S.Y., Xu, X., Zhou, X., 2002. Zircon chemistry and magma mixing, SE China: *in-situ* analysis of Hf isotopes, Tonglu and Pingtan igneous complexes. *Lithos* 61, 237–269.
- Griffin, W., Powell, W., Pearson, N., O'Reilly, S., 2008. GLITTER: data reduction software for laser ablation ICP-MS. *Laser Ablation-ICP-MS in the Earth Sciences. Mineralogical Association of Canada Short Course Series*, 40, pp. 204–207.
- Guan, H., Sun, M., Wilde, S.A., Zhou, X., Zhai, M., 2002. SHRIMP U–Pb zircon geochronology of the Fuping Complex: implications for formation and assembly of the North China Craton. *Precambrian Research* 113, 1–18.
- Guitreau, M., Blachert-Toft, J., Martin, H., Mojzsis, S.J., Albarède, F., 2012. Hafnium isotope evidence from Archean granitic rocks for deep-mantle origin of continental crust. *Earth and Planetary Science Letters* 337–338, 211–223.
- Hanchar, J.M., van Westrenen, W., 2007. Rare earth element behavior in zircon–melt systems. *Elements* 3, 37–42.
- Hand, M., Reid, A., Jagodzinski, L., 2007. Tectonic framework and evolution of the Gawler Craton, Southern Australia. *Economic Geology* 102, 1377–1395.
- Harley, S.L., Black, L.P., 1997. A revised Archean chronology for the Napier Complex, Enderby Land, from SHRIMP ion-microprobe studies. *Antarctic Science* 9, 74–91.
- Hofmann, A.E., Valley, J.W., Watson, E.B., Cavosie, A.J., Eiler, J.M., 2009. Sub-micron scale distributions of trace elements in zircon. *Contributions to Mineralogy and Petrology* 158, 317–335.
- Högdahl, K., Majka, J., Sjöström, H., Nilsson, K., Claesson, S., Konečný, P., 2011. Reactive monazite and robust zircon growth in diatexites and leucogranites from a hot, slowly cooled orogen: implications for the Palaeoproterozoic tectonic evolution of the central Fennoscandian Shield, Sweden. *Contributions to Mineralogy and Petrology* 1–22.
- Hokada, T., Misawa, K., Shiraishi, K., Suzuki, S., 2003. Mid to late Archean (3.3–2.5 Ga) tonalitic crustal formation and high-grade metamorphism at Mt. Riiser-Larsen, Napier Complex, East Antarctica. *Precambrian Research* 127, 215–228.
- Hollis, J.A., Beyer, E.E., Whelan, J.A., Kemp, A.I.S., Schersten, A., Greig, A., 2010. Summary of results: NTGS Laser U–Pb and Hf geochronology project: Pine Creek Orogen, Murphy Inlier, Arthur Basin and Arunta Region, July 2007–June 2008, Northern Territory Geological Survey.
- Horie, K., Hokada, T., Hiroi, Y., Motoyoshi, Y., Shiraishi, K., 2012. Contrasting Archean crustal records in western part of the Napier Complex, East Antarctica: new constraints from SHRIMP geochronology. *Gondwana Research* 21 (4), 829–837 (May).
- Hoskin, P.W.O., Black, L.P., 2000. Metamorphic zircon formation by solid-state recrystallization of protolith igneous zircon. *Journal of Metamorphic Geology* 18, 423–439.
- Hoskin, P.W.O., Schaltegger, U., 2003. The composition of zircon and igneous and metamorphic petrogenesis. In: Hanchar, J.M., Hoskin, P.W.O. (Eds.), *Zircon*, pp. 27–62.
- Hou, G., Santosh, M., Qian, X., Lister, G.S., Li, J., 2008. Configuration of the Late Palaeoproterozoic supercontinent Columbia: insights from radiating mafic dyke swarms. *Gondwana Research* 14, 395–409.
- Howard, K.E., Hand, M., Barovich, K.M., Payne, J.L., Belousova, E.A., 2011. U–Pb, Lu–Hf and Sm–Nd isotopic constraints on provenance and depositional timing of metasedimentary rocks in the western Gawler Craton: implications for Proterozoic reconstruction models. *Precambrian Research* 184, 43–62.
- Jackson, S.E., Pearson, N.J., Griffin, W.L., Belousova, E.A., 2004. The application of laser ablation-inductively coupled plasma-mass spectrometry to *in situ* U–Pb zircon geochronology. *Chemical Geology* 211, 47–69.
- Jayananda, M., Chardon, D., Peucat, J.J., Capdevila, R., 2006. 2.61 Ga potassic granites and crustal reworking in the western Dharwar craton, southern India: tectonic, geochronologic and geochemical constraints. *Precambrian Research* 150, 1–26.
- Jayananda, M., Moyen, J.F., Martin, H., Peucat, J.J., Autray, B., Mahabaleswar, B., 2000. Late Archean (2550–2520 Ma) juvenile magmatism in the Eastern Dharwar craton, southern India: constraints from geochronology, Nd–Sr isotopes and whole rock geochemistry. *Precambrian Research* 99, 225–254.
- Kelly, N.M., Clarke, G.L., Fanning, C.M., 2002. A two-stage evolution of the Neoproterozoic Rayner Structural Episode: new U–Pb sensitive high resolution ion microprobe constraints from the Oygarden Group, Kemp Land, East Antarctica. *Precambrian Research* 116, 307–330.
- Kelsey, D.E., Clark, C., Hand, M., 2008. Thermobarometric modelling of zircon and monazite growth in melt-bearing systems: examples using model metapelitic and metapsammitic granulites. *Journal of Metamorphic Geology* 26, 199–212.
- Kemp, A.I.S., Hawkesworth, C.J., Paterson, B.A., Kinny, P.D., 2006. Episodic growth of the Gondwana supercontinent from hafnium and oxygen isotopes in zircon. *Nature* 439, 580–583.
- Kinny, P.D., Friend, C.R.L., Strachan, R.A., Watt, G.R., Burns, I.M., 1999. U–Pb geochronology of regional migmatites in East Sutherland, Scotland: evidence for crustal melting during the Caledonian orogeny. *Journal of the Geological Society* 156, 1143–1152.
- Korhonen, F.J., Saw, A.K., Clark, C., Brown, M., Bhattacharya, S., 2011. New constraints on UHT metamorphism in the Eastern Ghats Province through the application of phase equilibria modelling and *in situ* geochronology. *Gondwana Research* 20, 764–781.
- Kovach, V.P., Simmat, R., Rickers, K., Bereznaya, N.G., Salnikova, E.B., Dobmeier, C., Raith, M.M., Yakovleva, S.Z., Kotov, A.B., 2001. The Western Charnockite Zone of the Eastern Ghats Belt, India – an Independent Crustal Province of Late Archean (2.8 Ga) and Palaeoproterozoic (1.7–1.6 Ga) Terrains. *Gondwana Research* 4, 666–667.
- Kretz, R., 1983. Symbols for rock-forming minerals. *American Mineralogist* 68, 277–279.
- Kröner, A., Wilde, S., Li, J., Wang, K., 2005. Age and evolution of a late Archean to Palaeoproterozoic upper lower crustal section in the Wutaishan/Hengshan/Fuping terrain of northern China. *Journal of Asian Earth Sciences* 24, 577–595.
- Kryza, R., Crowley, Q.G., Larionov, A., Pin, C., Oberc-Dziedzic, T., Mochnacka, K., 2012. Chemical abrasion applied to SHRIMP zircon geochronology: an example from the Variscan Karkonosze Granite (Sudetes, SW Poland). *Gondwana Research* 21 (4), 757–767.
- Kumar, K.V., Leelanandam, C., 2008. Evolution of the Eastern Ghats Belt, India: a plate tectonic perspective. *Journal of the Geological Society of India* 72, 720–749.
- Kumar, K.V., Ernst, W.G., Leelanandam, C., Wooden, J.L., Grove, M.J., 2010. First Palaeoproterozoic ophiolite from Gondwana: geochronologic–geochemical documentation of ancient oceanic crust from Kandra, SE India. *Tectonophysics* 487, 22–32.
- Lanyon, R., Black, L.P., Seitz, H.-M., 1993. U–Pb zircon dating of mafic dykes and its application to the Proterozoic geological history of the Vestfold Hills, East Antarctica. *Contributions to Mineralogy and Petrology* 115, 184–203.
- Leelanandam, C., 1997. The Kondapalli Layered Complex, Andhra Pradesh, India: a synoptic overview. *Gondwana Research* 1, 95–114.
- Liu, F., Guo, J., Lu, X., Diwu, C., 2009. Crustal growth at <2.5 Ga in the North China Craton: evidence from whole-rock Nd and zircon Hf isotopes in the Huai'an gneiss terrane. *Chinese Science Bulletin* 54, 4704–4713.
- Maidment, D.W., Hand, M., Williams, I.S., 2005. Tectonic cycles in the Strangways Metamorphic Complex, Arunta Inlier, central Australia: geochronological evidence for exhumation and basin formation between two high-grade metamorphic events\*. *Australian Journal of Earth Sciences* 52, 205–215.
- McGee, B., Giles, D., Kelsey, D.A., Collins, A.S., 2010. Protolith heterogeneity as a factor controlling the feedback between deformation, metamorphism and melting in a granulite-hosted gold deposit. *Journal of the Geological Society of London* 167, 1089–1104.
- Melletot, J., Faure, M., Cocherie, A., 2009. Monazite U–Th/Pb chemical dating of the Early Carboniferous syn-kinematic MP/MT metamorphism in the Variscan French Massif Central. *Bulletin de la Société Géologique de France* 180, 283–292.
- Mezger, K., Cosca, M.A., 1999a. The thermal history of the Eastern Ghats Belt (India) as revealed by U–Pb and  $^{40}\text{Ar}/^{39}\text{Ar}$  dating of metamorphic and magmatic minerals: implications for the SWEAT correlation. *Precambrian Research* 94, 251–271.
- Mezger, K., Cosca, M.A., 1999b. The thermal history of the Eastern Ghats Belt (India) as revealed by U–Pb and Ar-40/Ar-39 dating of metamorphic and magmatic minerals: implications for the SWEAT correlation. *Precambrian Research* 94, 251–271.
- Mohanty, S., 2011. Palaeoproterozoic assembly of the Napier Complex, Southern India and Western Australia: implications for the evolution of the Cuddapah basin. *Gondwana Research* 20, 344–361.
- Montel, Kornprobst, Vielzeuf, 2000. Preservation of old U–Th–Pb ages in shielded monazite: example from the Beni Boussera Hercynian kinzrites (Morocco). *Journal of Metamorphic Geology* 18, 335–342.
- Mukhopadhyay, D., Basak, K., 2009. The Eastern Ghats Belt – a polycyclic granulite terrain. *Journal of the Geological Society of India* 73, 489–518.
- Naqvi, S.M., 2005. Geology and Evolution of the Indian Plate: From Hadean to the Holocene. 4 Ga to 4 Ka. Capital Pub. Co., New Delhi.
- Owada, M., Osanai, Y., Toyoshima, T., Tsunogae, T., Hokada, T., Kagami, H., 2001. Late Archaean to proterozoic tectonothermal events in Napier Complex, East Antarctica: correlation with East Gondwana fragments. *Gondwana Research* 4, 724–725.
- Payne, J.L., Hand, M., Barovich, K.M., Wade, B.P., 2008. Temporal constraints on the timing of high-grade metamorphism in the northern Gawler Craton: implications for assembly of the Australian Proterozoic. *Australian Journal of Earth Sciences* 55, 623–640.
- Payne, J.L., Ferris, G., Barovich, K.M., Hand, M., 2010. Pitfalls of classifying ancient magmatic suites with tectonic discrimination diagrams: an example from the Palaeoproterozoic Tunkillia Suite, southern Australia. *Precambrian Research* 177, 227–240.
- Pidgeon, R.T., Nemchin, A.A., Hitchen, G.J., 1998. Internal structures of zircons from Archaean granites from the Darling Range batholith: implications for zircon stability and the interpretation of zircon U–Pb ages. *Contributions to Mineralogy and Petrology* 132, 288–299.
- Pisarevsky, S.A., Biswal, T.K., Wang, X.-C., De Waele, B., Ernst, R., Söderlund, U., Tait, J.A., Ratn, K., Singh, Y.K., Cleve, M., 2013. Palaeomagnetic, geochronological and geochemical study of Mesoproterozoic Lakhna Dykes in the Bastar Craton, India: implications for the Mesoproterozoic supercontinent. *Lithos* 174, 125–143 (1 August).

- Ramakrishnan, M., Vaidyanadhan, R., 2010. Geology of India Geological Society of India, Bangalore.
- Ramakrishnan, M., Nanda, J.K., Augustine, P.F., 1998. Geologic evolution of the Proterozoic Eastern Ghats Mobile Belt. Geological Survey of India Special Publication 44, 1–21.
- Ravikant, V., 2010. Palaeoproterozoic (1.9 Ga) extension and breakup along the eastern margin of the Eastern Dharwar Craton, SE India: new Sm–Nd isochron age constraints from anorogenic mafic magmatism in the Neoproterozoic Nellore greenstone belt. *Journal of Asian Earth Sciences* 37, 67–81.
- Rickers, K., Mezger, K., Raith, M.M., 2001. Evolution of the continental crust in the Proterozoic Eastern Ghats Belt, India and new constraints for Rodinia reconstruction: implications from Sm–Nd, Rb–Sr and Pb–Pb isotopes. *Precambrian Research* 112, 183–210.
- Roberts, M.P., Finger, F., 1997. Do U–Pb zircon ages from granulites reflect peak metamorphic conditions? *Geology* 25, 319–322.
- Rogers, J.J.W., Santosh, M., 2002. Configuration of Columbia, a Mesoproterozoic supercontinent. *Gondwana Research* 5, 5–22.
- Rubatto, D., 2002. Zircon trace element geochemistry: partitioning with garnet and the link between U–Pb ages and metamorphism. *Chemical Geology* 184, 123–138.
- Rubatto, D., Williams, I.S., Buick, I.S., 2001. Zircon and monazite response to prograde metamorphism in the Reynolds Range, central Australia. *Contributions to Mineralogy and Petrology* 140, 458–468.
- Saha, D., 2011. Dismembered ophiolites in Palaeoproterozoic nappe complexes of Kandra and Gurrakonda, South India. *Journal of Asian Earth Sciences* 42, 158–175.
- Santosh, M., Sajeew, K., Li, J.H., 2006. Extreme crustal metamorphism during Columbia supercontinent assembly: evidence from North China Craton. *Gondwana Research* 10, 256–266.
- Sarkar, A., Paul, D.K., 1998. Geochronology of the Eastern Ghats precambrian mobile belt—a review. *Geological Survey of India Special Publication* 44, 51–86.
- Schaltegger, U., Fanning, C., Günther, D., Maurin, J., Schulmann, K., Gebauer, D., 1999. Growth, annealing and recrystallization of zircon and preservation of monazite in high-grade metamorphism: conventional and in-situ U–Pb isotope, cathodoluminescence and microchemical evidence. *Contributions to Mineralogy and Petrology* 134, 186–201.
- Scherer, E., Müunker, C., Mezger, K., 2001. Calibration of the lutetium–hafnium clock. *Science* 293, 683–687.
- Segal, I., Halicz, L., Platzner, I.T., 2003. Accurate isotope ratio measurements of ytterbium by multiple collection inductively coupled plasma mass spectrometry applying erbium and hafnium in an improved double external normalization procedure. *Journal of Analytical Atomic Spectrometry* 18, 1217–1223.
- Sengupta, P., Sen, J., Dasgupta, S., Raith, M., Bhui, U.K., Ehl, J., 1999. Ultra-high temperature metamorphism of metapelitic granulites from Kondapalle, Eastern Ghats Belt: implications for the Indo-Antarctic correlation. *Journal of Petrology* 40, 1065–1087.
- Simmat, R., Raith, M., 1998. EPMA monazite dating of metamorphic events in the Eastern Ghats Belt of India. Berichte der Deutschen Mineralogischen Gesellschaft, Beihef zum European Journal of Mineralogy 10, 276.
- Simmat, R., Raith, M.M., 2008. U–Th–Pb monazite geochronometry of the Eastern Ghats Belt, India: timing and spatial disposition of poly-metamorphism. *Precambrian Research* 162, 16–39.
- Sláma, J., Kosler, J., Condon, D.J., Crowley, J.L., Gerdes, A., Hanchar, J.M., Horstwood, M.S.A., Morris, G.A., Nasdala, L., Norberg, N., Schaltegger, U., Schoene, B., Tubrett, M.N., Whitehouse, M.J., 2008. Plešovice zircon – a new natural reference material for U–Pb and Hf isotopic microanalysis. *Chemical Geology* 249, 1–35.
- Suzuki, S., Arima, M., Williams, I.S., Shiraishi, K., Kagami, H., 2006. Thermal History of UHT Metamorphism in the Napier Complex, East Antarctica: insights from Zircon, Monazite, and Garnet ages. *Journal of Geology* 114, 65–84.
- Swain, G., Woodhouse, A., Hand, M., Barovich, K., Schwarz, M., Fanning, C.M., 2005. Provenance and tectonic development of the late Archaean Gawler Craton, Australia: U–Pb zircon, geochemical and Sm–Nd isotopic implications. *Precambrian Research* 141, 106–136.
- Tichomirowa, M., Whitehouse, M.J., Nasdala, L., 2005. Resorption, growth, solid state recrystallisation, and annealing of granulite facies zircon—a case study from the Central Erzgebirge, Bohemian Massif. *Lithos* 82, 25–50.
- Upadhyay, D., Gerdes, A., Raith, M.M., 2009. Unraveling sedimentary provenance and tectonothermal history of high-temperature metapelites, using zircon and monazite chemistry: a case study from the Eastern Ghats Belt, India. 117, 665–683.
- Vadlamani, R., Kröner, A., Vasudevan, D., Wendt, I., Tobschall, H., Chatterjee, C., 2012. Zircon evaporation ages and geochemistry of metamorphosed volcanic rocks from the Vinjamuru domain, Krishna Province: evidence for 1.78 Ga convergent tectonics along the southeastern margin of the Eastern Dharwar Craton. *Geological Journal* 48 (4), 293–309.
- Van Achterbergh, E., R.C.G., Jackson, S.E., Griffin, W.L., 2001. Appendix 3: data reduction software for LA-ICP-MS. In: Sylvester, P. (Ed.), *Laser-Ablation-ICPMS in the Earth Sciences*. Mineralogical Association of Canada, pp. 239–243.
- Vervoort, J.D., Patchett, P.J., Söderlund, U., Baker, M., 2004. Isotopic composition of Yb and the determination of Lu concentrations and Lu/Hf ratios by isotope dilution using MC-ICPMS. *Geochemistry, Geophysics, Geosystems* 5, Q11002.
- Vijaya Kumar, K., Ernst, W.G., Leelanandam, C., Wooden, J.L., Grove, M.J., 2010. First Palaeoproterozoic ophiolite from Gondwana: geochronologic-geochemical documentation of ancient oceanic crust from Kandra, SE India. *Tectonophysics* 487, 22–32.
- Vijaya Kumar, K., Leelanandam, C., Ernst, W.G., 2011. Formation and fragmentation of the Palaeoproterozoic supercontinent Columbia: evidence from the Eastern Ghats Granulite Belt, southeast India. *International Geology Review* 53, 1297–1311.
- Wan, Y., Liu, D., Dong, C., Liu, S., Wang, S., Yang, E., 2011. U–Th–Pb behavior of zircons under high-grade metamorphic conditions: a case study of zircon dating of meta-diorite near Qixia, eastern Shandong. *Geoscience Frontiers* 2, 137–146.
- Wang, Y., Zhao, G., Fan, W., Peng, T., Sun, L., Xia, X., 2007. LA-ICP-MS U–Pb zircon geochronology and geochemistry of Paleoproterozoic mafic dykes from western Shandong Province: implications for back-arc basin magmatism in the Eastern Block, North China Craton. *Precambrian Research* 154, 107–124.
- Woodhead, J., Hergt, J., Shelley, M., Eggins, S., Kemp, R., 2004. Zircon Hf-isotope analysis with an excimer laser, depth profiling, ablation of complex geometries, and concomitant age estimation. *Chemical Geology* 209, 121–135.
- Xiang, W., Griffin, W.L., Jie, C., Pinyun, H., Xiang, Ll., 2011. U and Th contents and Th/U ratios of zircon in felsic and mafic magmatic rocks: improved zircon-melt distribution coefficients. *Acta Geologica Sinica – English Edition* 85, 164–174.
- Yin, C., Zhao, G., Guo, J., Sun, M., Xia, X., Zhou, X., Liu, C., 2011. U–Pb and Hf isotopic study of zircons of the Helanshan Complex: constrains on the evolution of the Khondalite Belt in the Western Block of the North China Craton. *Lithos* 122, 25–38.
- Zeh, A., Williams, I., Brätz, H., Millar, I., 2003. Different age response of zircon and monazite during the tectono-metamorphic evolution of a high grade paragneiss from the Ruhla Crystalline Complex, central Germany. *Contributions to Mineralogy and Petrology* 145, 691–706.
- Zhai, M.-G., Santosh, M., 2011. The early Precambrian odyssey of the North China Craton: a synoptic overview. *Gondwana Research* 20, 6–25.
- Zhai, M., Li, T.-S., Peng, P., Hu, B., Liu, F., Zhang, Y., 2010. Precambrian key tectonic events and evolution of the North China Craton. *Geological Society, London, Special Publications* 338, 235–262.
- Zhang, S.B., Zheng, Y.F., Wu, Y.B., Zhao, Z.F., Gao, S., Wu, F.Y., 2006. Zircon U–Pb age and Hf–O isotope evidence for Palaeoproterozoic metamorphic event in South China. *Precambrian Research* 151, 265–288.
- Zhang, Shuan-Hong, Liu, Shu-Wen, Zhao, Yue, Yang, Jin-Hui, Song, Biao, Liu, Xiao-Ming, 2007. The 1.75–1.68 Ga anorthosite–mangerite–alkali granitoid–rapakivi granite suite from the northern North China Craton: magmatism related to a Paleoproterozoic orogen. *Precambrian Research* 155 (3–4), 287–312. <http://dx.doi.org/10.1016/j.precamres.2007.02.008>.
- Zhang, S., Li, Z.-X., Evans, D.A.D., Wu, H., Li, H., Dong, J., 2012. Pre-Rodinia supercontinent Nuna shaping up: a global synthesis with new palaeomagnetic results from North China. *Earth and Planetary Science Letters* 353–354, 145–155.
- Zhao, J.-X., Bennett, V.C., 1995. SHRIMP U–Pb zircon geochronology of granites in the Arunta Inlier, central Australia: implications for Proterozoic crustal evolution. *Precambrian Research* 71, 17–43.
- Zhao, G.C., Cawood, P.A., Wilde, S.A., Sun, M., 2002. Review of global 2.1–1.8 Ga orogens: implications for a pre-Rodinia supercontinent. *Earth-Science Reviews* 59, 125–162.
- Zhao, G.C., Sun, M., Wilde, S.A., Li, S.Z., 2004. A Palaeo-Mesoproterozoic supercontinent: assembly, growth and breakup. *Earth-Science Reviews* 67, 91–123.